Nonlinear Dyn
https://doi.org/10.1007/s11071-025-11161-9

RESEARCH

# Adaptive predefined time tracking control for nonlinear multi-agent systems subject to input saturation: an improved command filtering approach

**Wei-Jie Hao · Jing-Jing Sun · Zhao-Yi Zong · Shan-Liang Zhu · Yu-Qun Han**

Received: 22 January 2025 / Accepted: 23 March 2025


**Abstract** This paper presents a practical predefined time control approach for nonlinear multi-agent systems with input saturation. A novel predefined time command filter, constructed using a hyperbolic tangent function, effectively addresses the issues of computational explosion problems and control singularity commonly observed in traditional backstepping designs. To enhance control precision and robustness, a filter compensation signal is introduced to mitigate errors caused by the command filter. Furthermore, a new injective and differentiable function is developed by integrating the properties of horizontal and oblique asymptotes, providing an effective solution for managing input saturation. Leveraging this foundation, a predefined time command filtering controller is designed by combining adaptive backstepping control with the multi-dimensional Taylor network technique, which significantly simplifies the controller design process. Utilizing practically predefined time stable theory, the boundedness of all closed-loop system signals is rigorously established, and it is proven that synchronization errors converge to a small neighborhood around the origin within the predefined time. Finally, simulation results validate the proposed method's effectiveness and practical applicability.

**Keywords** Multi-agent systems · Multi-dimensional Taylor networks · Predefined time control · Command filter · Input saturation · Adaptive control

## 1 Introduction

Over the past two decades, multi-agent systems (MASs) have gained significant attention due to their extensive applications in distributed optimization [1], smart grids [2], artificial intelligence [3], and robotics [4]. Consensus problems in MASs are generally categorized into leaderless consensus [5,6] and leader-follower consensus, depending on the presence of a leader. Significant progress has been achieved in leader-follower consensus for first-order MASs [7], second-order MASs [8], and high-order MASs [9]. However, most existing studies primarily focus on linear MASs or basic NMASs. For MASs with unknown dynamics or nonlinearly parameterized uncertainties, techniques such as fuzzy control [10–12], neural networks [13,14], and multi-dimensional Taylor network (MTN) [15,16] combined with adaptive backstepping have been developed to address these challenges. In traditional backstepping methods, the repeated differentiation of virtual control laws often leads to computational explosion. Dynamic surface control (DSC) [17] was introduced to mitigate this issue by using first-order filters

W.-J. Hao · J.-J. Sun · Z.-Y. Zong · S.-L. Zhu · Y.-Q. Han
School of Mathematics and Physics, Qingdao University of Science and Technology, Qingdao 266061, China

W.-J. Hao · J.-J. Sun · Z.-Y. Zong · S.-L. Zhu · Y.-Q. Han (✉)
Qingdao Innovation Center of Artificial Intelligence Ocean Technology, Qingdao 266061, China
e-mail: yuqunhan@qust.edu.cn

Published online: 15 April 2025

to approximate the derivatives of virtual control laws. Subsequently, command filtering techniques incorporating error-compensating signals [18] were developed to reduce filtering errors and improve the precision of virtual control law approximations. Among various tools, MTN-a specialized neural network characterized by a simple structure and strong approximation capabilities-has proven effective in addressing nonlinear system challenges. However, its application to NMASs with input saturation remains unexplored, serving as a key motivation for this study.

Convergence speed is a critical metric in evaluating system tracking performance. Asymptotic tracking control [19] improves convergence speed but guarantees convergence only asymptotically, resulting in infinite convergence time, which is impractical for systems requiring strict timing constraints. Finite-time control [20,21], offering rapid convergence and strong disturbance rejection, has become prominent in engineering applications. However, the convergence time of finite-time control depends on the initial state deviation, potentially approaching infinity for large deviations. To overcome this limitation, fixed-time control [22] was developed, ensuring convergence time is independent of initial conditions and determined solely by controller parameters. Despite its advantages, fixed-time control introduces design complexity due to its dependence on multiple parameters. Predefined time control [23], which guarantees stability within a user-specified time regardless of initial conditions, has gained traction for its simplicity and applicability. It has been widely applied to uncertain nonlinear systems [24,25], switched nonlinear systems [26], and NMASs [27–29]. However, predefined time control faces singularity issues when synchronization errors approach zero. Existing methods address these issues using sign functions [15] and sliding mode control [29], but innovative solutions to these challenges remain a key research focus.

In industrial systems, input saturation, caused by actuator limitations, is unavoidable and significantly impacts performance and stability [30–32]. Current approaches to addressing input saturation include constructing auxiliary systems to generate compensatory signals [33–35] or approximating saturation functions with smooth functions, transforming the problem into one involving linear models with bounded errors. The latter approach is widely preferred due to its reduced computational complexity and simplified controller design, making it suitable for stochastic nonlinear systems [36,37], switched nonlinear systems [38], and NMASs [39,40]. Nevertheless, traditional smooth functions often exhibit complexity and susceptibility to high-frequency oscillations, underscoring the need to develop a novel smooth function as one of the primary objectives of this research.

Building on this background, this study proposes an adaptive predefined time MTN command filtering control method for NMASs with input saturation. The proposed method integrates both static and dynamic control performance. Its key contributions are summarized as follows:

(1) Conventional predefined time control techniques typically address singularity issues by employing sign functions or sliding mode surfaces. However, these methods often lead to undesirable control discontinuities and chattering. In contrast to the approach presented in [15], this study introduces an innovative predefined time command filter that integrates hyperbolic tangent functions with predefined time control theory. This novel filter ensures predefined time stability, effectively alleviating control singularities and avoiding computational explosions. Simulation comparison experiments validate the effectiveness of this approach. Unlike the first-order filters used in [28], the proposed filter eliminates the need for continuous differentiation of virtual control laws during the adaptive backstepping process, thus reducing complexity. Furthermore, it mitigates filtering errors through the use of compensatory signals. Additionally, while [29] is limited to second-order multi-agent systems (MASs), this work extends the methodology to disturbed high-order nonlinear multi-agent systems, significantly enhancing robustness and expanding the applicability of the proposed control scheme.
(2) Building upon the designed predefined time command filter, this paper presents a novel predefined time control scheme for nonlinear multi-agent systems. The proposed method explicitly integrates the desired convergence time into the controller design, enabling the user to set the system's establishment time independently of the initial conditions. This scheme not only effectively resolves the issue of convergence time dependence on initial states in finite-time control [21] but also eliminates the complexity of parameter design inherent in fixed-time

control [41]. Furthermore, it reduces conservatism and significantly enhances the robustness and practical applicability of the controller when handling complex scenarios, such as nonlinear dynamics and input saturation, within nonlinear multi-agent systems.

(3) To address the complexity and high-frequency oscillations associated with traditional Gaussian functions, this study constructs a smooth injective function combining horizontal and slanted asymptotes to approximate input saturation functions. By incorporating the inverse function of the virtual control law, the controller design achieves a simpler and more efficient structure. Moreover, this is the first application of MTN to NMASs with input saturation, leveraging its simple structure and strong approximation capabilities to simplify controller design further.

## 2 Problem description and preliminaries

### 2.1 Graph theory

In this study, the communication topology of the nonlinear multi-agent system is modeled as a directed graph $\mathcal{G}=(\mathcal{V},\mathcal{D},\mathcal{A})$, where $\mathcal{V}=\{1,\ldots,N\}$ represents the set of nodes, $\mathcal{D}$ denotes the set of edges, and $\mathcal{A}=\left[a_{i,j}\right]\in\Re^{N\times N}$ is the adjacency matrix that characterizes the communication between nodes. Specifically, $a_{i,j}>0$ if node $i$ can receive information from node $j$, and $a_{i,j}=0$ otherwise. If $a_{i,j}>0$, node $j$ is referred to as a neighbor of node $i$. The degree of node $i$ is defined as $a_i=\sum_{j=1}^{N}a_{i,j}$. The Laplacian matrix of the graph is defined as $\mathcal{L}=\mathcal{D}-\mathcal{A}$, where $\mathcal{D}=\mathrm{diag}\,(a_1,\ldots,a_N)$. In leader-follower MASs, the communication between the leader and followers is expressed through a matrix $\mathcal{B}=\mathrm{diag}\,(b_i)$, where $b_i>0$ indicates that the follower $i$ can receive signals from the leader, and $b_i=0$ otherwise.

### 2.2 System description

This study investigates a class of strict-feedback NMASs with input saturation. The dynamic model is expressed as

$$\begin{cases}\dot{x}_{i,j}=x_{i,j+1}+f_{i,j}\left(\bar{\boldsymbol{x}}_{i,j}\right)+d_{i,j}(t)\\ \dot{x}_{i,n}=h_{i,n}\left(\bar{\boldsymbol{x}}_{i,n}\right)u_i+f_{i,n}\left(\bar{\boldsymbol{x}}_{i,n}\right)+d_{i,n}(t)\\ y_i=x_{i,1},\,i=1,\ldots,N,\,j=1,\ldots,n\\ u_i=u_i(v_i(t))\end{cases}\tag{1}$$

where $\bar{\boldsymbol{x}}_{i,j}=\left[x_{i,1},x_{i,2},\cdots,x_{i,j}\right]^{\mathrm{T}}\in\Re^{j}$ is the state vector of the $i$-th follower, $u_i\in\Re$ and $y_i\in\Re$ are its input and output, respectively. The function $f_{i,j}\left(\bar{\boldsymbol{x}}_{i,j}\right)$ is an unknown smooth function satisfying the condition $f_{i,j}\left(\mathbf{0}\right)=0$. $u_i(v_i(t))$ represents the input saturation model (to be defined later), and $d_{i,j}(t)$ denotes unknown external disturbances satisfying $\left|d_{i,j}(t)\right|<\bar{d}_{i,j}$, with $\bar{d}_{i,j}>0$ being an unknown constant.

**Assumption 1** [42]. The nonlinear function $h_{i,n}\left(\bar{\boldsymbol{x}}_{i,n}\right)$ is unknown, but its sign is known. Positive constants $a_{i,m}$, $a_{i,M}$ exist such that $a_{i,m}<h_{i,n}\left(\bar{\boldsymbol{x}}_{i,n}\right)<a_{i,M}$. Without loss of generality, it is assumed that $h_{i,n}\left(\bar{\boldsymbol{x}}_{i,n}\right)>0$.

The leader's reference signal is given by

$$\dot{y}_d=f(y_d,t)\tag{2}$$

where $y_d$ is the leader's output, and $f(y_d,t)$ is a known function.

**Assumption 2** [43]. The leader's reference signal $y_d$ is $n$-th order continuously differentiable and bounded.

The synchronization error of the $i$-th follower is defined as

$$e_i=A_i(y_i-y_j)+b_i(y_i-y_d)\tag{3}$$

where $A_i=\sum_{j=1}^{N}a_{i,j}$. Additionally, $b_i=1$ if the $i$-th follower is able to receive signals from the leader, and $b_i=0$ otherwise.

**Assumption 3** [44]. The communication graph $\mathcal{G}$ includes a spanning tree with the leader node serving as the root.

**Lemma 1** *[16]: If Assumption 3 holds, then* $\mathcal{L}+\mathcal{B}>0$.

**Control Objective:** By selecting predefined time $T_p$ and parameters $\gamma$, an adaptive command-filtered controller based on the MTN framework is designed to ensure the following objectives:

(1) All signals in the closed-loop system are guaranteed to remain bounded.
(2) The tracking error converges to a small neighborhood of the origin within a predefined time.

### 2.3 Practical predefined time stability

Consider the following nonlinear system

$$\dot{x} = f(\boldsymbol{x}) \tag{4}$$

where the origin is assumed to be the equilibrium point of the system. Here, $\boldsymbol{x} \in \Re^n$ represents the system's state vector satisfying $x(\mathbf{0}) = x_0$, and $f(\boldsymbol{x}) : \Re^n \to \Re^n$ is a smooth function.

**Definition 1** [45]. For a predefined time $T_p > 0$, if there exists a constant $\varepsilon$ such that the solution $x(x_0, t)$ of system (4) satisfies $\|x(x_0, t)\| < \varepsilon$ for all $t \geq T_p$, then the origin of system (4) is said to exhibit practical predefined time stability.

**Lemma 2** *[25]: For system (4), there exists a radially unbounded positive definite function $V(x)$ such that the solution satisfies*

$$\dot{V} \leq -\frac{3\pi}{2\gamma T_p}\left(V^{1+\frac{\gamma}{2}} + V^{1-\frac{\gamma}{2}}\right) + \sigma \tag{5}$$

*where $T_p > 0$, $0 < \gamma < 1$, and $\sigma > 0$ are constants. Thus, system (4) is practically predefined time stable. Futhermore, for $t \geq T_p$, the system's solution $x(x_0, t)$ satisfies $V(x) \leq \frac{2\gamma T_p \sigma}{3\pi}$.*

**Lemma 3** *[25]: For any $x \in \Re$, $\mu > 0$, $k = 0.2785$, the following inequality holds*

$$0 \leq |x| - x\tanh\left(\frac{x}{\mu}\right) \leq k\mu \tag{6}$$

**Lemma 4** *[15]: For $x_i \in \Re$, $p > 1$, $q < 1$, $i = 1, \ldots, n$, the following inequality holds*

$$\left(\sum_{i=1}^{n} x_i\right)^q \leq \sum_{i=1}^{n} x_i^q \tag{7}$$

$$\left(\sum_{i=1}^{n} x_i\right)^p \leq n^{p-1}\left(\sum_{i=1}^{n} x_i^p\right) \tag{8}$$

**Lemma 5** *[28]: For $x \in \Re$, $y \in \Re$ and constants $c > 0$, $d > 0$, $\Phi > 0$, the following inequality holds*

$$|x|^c|y|^d \leq \frac{c}{c+d}\Phi|x|^{c+d} + \frac{d}{c+d}\Phi^{-\frac{c}{d}}|y|^{c+d} \tag{9}$$

**Lemma 6** *[46]: For $p \geq q$, $\eta > 1$, the following holds*

$$q(p-q)^\eta \leq \frac{\eta}{1+\eta}\left(p^{1+\eta} - q^{1+\eta}\right) \tag{10}$$

**Lemma 7** *[46]: Consider the following differential equation*

$$\dot{H}(t) = -aH(t) - bH^s(t) + c\varpi(t) \tag{11}$$

*where $a > 0$, $b > 0$, $c > 0$, $s = \frac{2n+k}{2n+1} > 1$, $k > 1$, $\varpi(t) > 0$ is a positive function and for any $t \geq t_0$, if the initial condition satisfies $H(t_0) > 0$, then $H(t) > 0$.*

### 2.4 Input saturation model

This study considers the following input saturation model

$$u_i(v_i(t), k_i) = \begin{cases} k_i c_i, & v_i(t) < c_i \\ k_i v_i(t), & c_i \leq v_i(t) \leq b_i \\ k_i b_i, & v_i(t) > b_i \end{cases} \tag{12}$$

where $c_i < 0$ and $b_i > 0$ denote the upper and lower bounds of the saturation function, respectively, and $k_i > 0$ is a constant. To approximate the saturation function, a smooth function is designed based on the principles of horizontal and oblique asymptotes

$$u_{im}(v_i(t)) = \begin{cases} r_{c_i} + \dfrac{v_i(t) - r_{c_i}}{1 + r_{c_i} - v_i(t)}, & v_i(t) < r_{c_i} \\ v_i(t), & r_{c_i} \leq v_i(t) \leq r_{b_i} \\ r_{b_i} + \dfrac{v_i(t) - r_{b_i}}{1 - r_{b_i} + v_i(t)}, & v_i(t) > r_{b_i} \end{cases} \tag{13}$$

where $r_{c_i} < 0$ and $r_{b_i} > 0$ are constants.

**Lemma 8** *Given that $u_{im}(v_i(t), k_i)$ is an injective and differentiable function, there exists a constant $M_i > 0$ such that*

$$u_i(v_i(t)) = k_{i1}u_{im}(v_i(t)) + \delta_i(v_i(t)) \tag{14}$$

*where $\delta_i(v_i(t)) \leq M_i$ and $k_i > k_{i1} > 0$.*

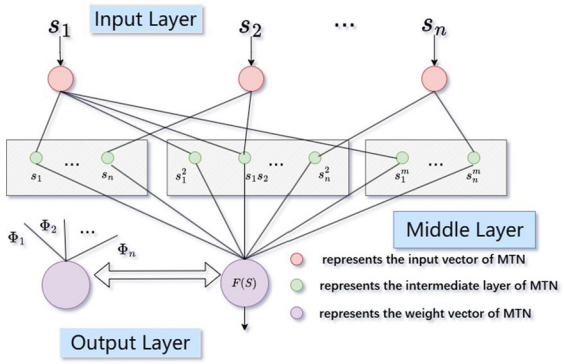


**Fig. 1** The structure of MTN

*Remark 1* Currently, two main approaches exist for addressing input saturation: one involves approximating the saturation function using smooth functions, while the other mitigates the effects of input saturation by constructing an auxiliary system. Inspired by horizontal and oblique asymptotes, this paper introduces a novel injective differentiable function to approximate the non-smooth, nonlinear input saturation function. This approach avoids the complexity of traditional smooth functions (such as Gaussian and Nussbaum functions). Furthermore, the inverse function of the virtual control law in backstepping design is employed for controller design, which not only reduces computational effort but also simplifies the controller design process.

### 2.5 Multi-dimensional Taylor network (MTN)

The multi-dimensional Taylor network (MTN) is utilized in this study to estimate the unknown nonlinear dynamics of the system. The MTN, a specialized neural network, consists of an input layer, hidden layers, and an output layer. The theoretical foundations and application concepts of MTN have been comprehensively detailed in [47,48], which also proposes the following lemma. The control structure of MTN is shown in Fig. 1.

**Lemma 9** *[47]: On a compact set* $\Omega \subset \Re^n$*, a continuous nonlinear function* $F(\boldsymbol{S}) : \Re^n \to \Re$ *can be approximated by the MTN as follows*

$$F(\boldsymbol{S}) = \boldsymbol{\Phi}^{\mathrm{T}} \boldsymbol{\xi}_{m_n}(\boldsymbol{S}) + \delta(\boldsymbol{S}) \tag{15}$$

*where* $\boldsymbol{S} = [s_1, s_2, \ldots, s_n]^{\mathrm{T}} \subset \Re^n$ *and* $\boldsymbol{\Phi} = [\boldsymbol{\Phi}_1, \boldsymbol{\Phi}_2, \ldots, \boldsymbol{\Phi}_l]^{\mathrm{T}} \subset \Re^l$ *represent input vector and the weight vector the MTN, respectively.* $\boldsymbol{\xi}_{m_n}(\boldsymbol{S}) = \left[s_1, s_2, \ldots, s_n, s_1^2, s_1 s_2, \ldots, s_n^2, \ldots, s_1^m, \ldots, s_n^m\right]^{\mathrm{T}} \subset \Re^l$ *denotes the intermediate layer of the MTN.* $\delta(\boldsymbol{S})$ *is the approximation error, and* $|\delta(\boldsymbol{S})| \leq \varepsilon$*, where* $\varepsilon$ *is a positive constant.*

*Remark 2* Multi-dimensional Taylor Network (MTN), similar to the Radial Basis Function Neural Network (RBFNN), consists of three layers: an input layer, a middle layer, and an output layer. However, unlike the RBFNN, which uses Gaussian functions in its middle layer, MTN utilizes a set of polynomials. This substitution simplifies the network structure and significantly lowers computational complexity.

*Remark 3* Although the nine lemmas presented in this paper are essential, they do not introduce significant conservatism into its findings. These lemmas primarily serve as tools that facilitate the development of the theory, providing both theoretical foundations and necessary support for subsequent derivations and analyses. Consequently, despite their relatively large number, their main purpose is to strengthen the credibility and reliability of the research, rather than to add conservatism.

## 3 Controller design and stability analysis

### 3.1 Predefined time command filter design

To improve the tracking performance of MASs and ensure synchronization errors converge within a predefined time, a command filter design method based on predefined time is proposed. The specific design steps are as follows.

First, the following coordinate transformation is defined

$$\begin{cases} s_{i,1} = e_i = A_i(y_i - y_j) + b_i(y_i - y_d) \\ s_{i,j} = x_{i,j} - \omega_{i,j},\ j = 1, \ldots, n \end{cases} \tag{16}$$

where $s_{i,j}$ represents the tracking error of the follower, and $\omega_{i,j}$ is the output signal of the command filter.

To further minimize tracking errors, the filtering error is defined as

$$\varphi_{i,j} = \omega_{i,j} - \alpha_{i,j-1} \tag{17}$$

where $j = 2, 3, \ldots n$, and $\alpha_{i,j-1}$ is the virtual control signal to be designed.

To guarantee synchronization error convergence within a predefined time, the predefined time command filter is designed as

$$\begin{cases} \omega_{i,j}(0) = \alpha_{i,j-1}(0) \\ \dot{\omega}_{i,j} = -\dfrac{3\pi}{2\gamma T_p}\varphi_{i,j}^{1+\gamma}\lambda \tanh\left(\dfrac{3\pi}{2\gamma T_p}\lambda\dfrac{\varphi_{i,j}^{2+\gamma}}{\varepsilon_{i,j}}\right) \\ \qquad -\upsilon_{i,j}\varphi_{i,j} \\ \qquad -\dfrac{3\pi}{2\gamma T_p}\varphi_{i,j}^{1-\gamma}\bar{\lambda}\tanh\left(\dfrac{3\pi}{2\gamma T_p}\bar{\lambda}\dfrac{\varphi_{i,j}^{2-\gamma}}{\varepsilon_{i,j}}\right) \end{cases} \tag{18}$$

where $\lambda = \left(\frac{1}{2}\right)^{1+\frac{\gamma}{2}}(n-1)^{\frac{\gamma}{2}}$, $\bar{\lambda} = \left(\frac{1}{2}\right)^{1-\frac{\gamma}{2}}$, $\gamma > 0$, $\upsilon_{i,j} > 0$ are design parameters, and $T_p$ is the predefined time ensuring error convergence within this period.

*Remark 4* In predefined time control, singularity issues are typically addressed using the sign function and sliding mode surfaces. In contrast, this paper proposes a predefined time command filter based on the hyperbolic tangent function, utilizing the properties of hyperbolic functions. The design of this filter ensures that the virtual control function, control input, and parameter adaptation law remain continuous and free from singularities. This approach effectively mitigates control discontinuities and chattering, which are commonly encountered in traditional predefined time control methods. Furthermore, it provides an innovative solution to the singularity problem in predefined time control for nonlinear multi-agent systems. The authors in [25] considers a nonlinear system, which can be viewed as a special case of the scenario discussed in this paper, where only one follower agent is selected.

Since practical systems may exhibit significant errors due to the filter, a compensating error signal $z_{i,j}$ $(j = 1, \ldots, n)$ is defined to address this potential deviation

$$z_{i,j} = s_{i,j} - Q_{i,j} \tag{19}$$

The compensating signal $Q_{i,j}$ is specifically expressed as

$$\begin{cases} \dot{Q}_{i,1} = (A_i + b_i)\left(-\dfrac{c_{i,1}Q_{i,1}}{A_i + b_i} + Q_{i,2} + \omega_{i,2} - \alpha_{i,1}\right) \\ \dot{Q}_{i,2} = Q_{i,3} + \omega_{i,3} - \alpha_{i,2} - (A_i + b_i)\,Q_{i,1} - c_{i,2}Q_{i,2} \\ \dot{Q}_{i,j} = Q_{i,j+1} + \omega_{i,j+1} - \alpha_{i,j} - Q_{i,j-1} - c_{i,j}Q_{i,j} \\ \quad j = 3, \ldots, n-1 \\ \dot{Q}_{i,n} = -k_{i1}\left(Q_{i,n-1} + c_{i,n}Q_{i,n}\right) \end{cases} \tag{20}$$

where $c_{i,j} > 0$ is a constant that adjusts the compensating signal's gain.

Finally, the derivative of the compensating error signal $z_{i,j}$ $(j = 1, \ldots, n)$ is derived as follows

$$\begin{aligned} \dot{z}_{i,1} = {} & (A_i + b_i)\left(z_{i,2} + f_{i,1} + d_{i,1} + \alpha_{i,1}\right) - b_i\dot{y}_d \\ & - A_i\left(x_{j,2} + f_{j,1} + d_{j,1}\right) + c_{i,1}Q_{i,1} \end{aligned} \tag{21}$$

### 3.2 Controller design

*Step 1:* First, the candidate Lyapunov function $V_{i,1}$ is defined as

$$V_{i,1} = \sum_{i=1}^{N}\left(\frac{1}{2}z_{i,1}^2 + \frac{1}{2}\tilde{H}_{i,1}^2\right) \tag{22}$$

where $H_{i,1} = \max\left\|\boldsymbol{\Phi}_{i,1}\right\|^2 \geq 0$, $\tilde{H}_{i,1} = H_{i,1} - \hat{H}_{i,1}$, $\hat{H}_{i,1}$ is the estimations of $H_{i,1}$. According to *Lemma 7*, it is evident that $\hat{H}_{i,1} \geq 0$.

By differentiating the Lyapunov function, we obtain

$$\begin{aligned} \dot{V}_{i,1} = \sum_{i=1}^{N}\Big[ & z_{i,1}((A_i + b_i)\left(z_{i,2} + f_{i,1} + d_{i,1} + \alpha_{i,1}\right) \\ & - A_i\left(x_{j,2} + f_{j,1} + d_{j,1}\right) - b_i\dot{y}_d + c_{i,1}Q_{i,1}) \\ & - \tilde{H}_{i,1}\dot{\hat{H}}_{i,1}\Big] \end{aligned} \tag{23}$$

Using the Young's inequality, the following can be further derived

$$z_{i,1}\,(A_i + b_i)\,d_{i,1} \leq \frac{1}{2}(A_i + b_i)^2 z_{i,1}^2 + \frac{1}{2}\bar{d}_{i,1}^2 \tag{24}$$

$$-z_{i,1}A_i d_{j,1} \leq \frac{1}{2}A_i^2 z_{i,1}^2 + \frac{1}{2}\bar{d}_{j,1}^2 \tag{25}$$

Choosing $F_{i,1} = f_{i,1} - \frac{A_i}{A_i+b_i}\left(f_{j,1}+x_{j,2}\right) - \frac{b_i}{A_i+b_i}\dot{y}_d + z_{i,1}\left(A_i+b_i\right) + \frac{1}{2}\frac{A_i^2}{(A_i+b_i)}z_{i,1}$, and based on *Lemma 9*, the unknown functions are approximated using the MTN approach. Additionally, by applying the Young's inequality, we have

$$\begin{aligned} z_{i,1}\left(A_i+b_i\right)F_{i,1} &= z_{i,1}\left(A_i+b_i\right)\boldsymbol{\Phi}_{i,1}^{\mathrm{T}}\boldsymbol{\xi}_{i,1} \\ &\quad + z_{i,1}\left(A_i+b_i\right)\delta_{i,1} \\ &\le \frac{1}{2p_{i,1}^2}z_{i,1}^2(A_i+b_i)^2H_{i,1}\boldsymbol{\xi}_{i,1}^{\mathrm{T}}\boldsymbol{\xi}_{i,1} \\ &\quad + \Lambda_{i,1} + \frac{1}{2}z_{i,1}^2(A_i+b_i)^2 \end{aligned} \tag{26}$$

where $p_{i,1} > 0$ is a constant, $\Lambda_{i,1} = \frac{1}{2}p_{i,1}^2 + \frac{1}{2}\varepsilon_{i,1}^2$.

Substituting Eqs. (24), (25), and (26) into (23), the following is obtained

$$\begin{aligned} \dot{V}_{i,1} \le \sum_{i=1}^{N}\Bigg[ & z_{i,1}\left[\left(A_i+b_i\right)\left(z_{i,2}+\alpha_{i,1}\right)\right] \\ & + \Lambda_{i,1} + \frac{1}{2}\bar{d}_{i,1}^2 \\ & + \frac{1}{2p_{i,1}^2}z_{i,1}^2\left(A_i+b_i{}^2\right)H_{i,1}\boldsymbol{\xi}_{i,1}^{\mathrm{T}}\boldsymbol{\xi}_{i,1} + \frac{1}{2}\bar{d}_{j,1}^2 \\ & - \tilde{H}_{i,1}\dot{\hat{H}}_{i,1} + z_{i,1}c_{i,1}Q_{i,1}\Bigg] \end{aligned} \tag{27}$$

According to (27), the predefined time virtual control law $\alpha_{i,1}$ and adaptive law $\dot{\hat{H}}_{i,1}$ are designed as follows

$$\begin{aligned} \alpha_{i,1} = \frac{1}{A_i+b_i}\Bigg( & -\frac{3\pi}{2\gamma T_p}z_{i,1}^{1+\gamma}\chi\tanh\left(\frac{3\pi}{2\gamma T_p}\chi\frac{z_{i,1}^{2+\gamma}}{\mu_{i,1}}\right) \\ & - \frac{3\pi}{2\gamma T_p}z_{i,1}^{1-\gamma}\bar{\chi}\tanh\left(\frac{3\pi}{2\gamma T_p}\bar{\chi}\frac{z_{i,1}^{2-\gamma}}{\mu_{i,1}}\right) \\ & - \frac{1}{2p_{i,1}^2}z_{i,1}(A_i+b_i)^2\hat{H}_{i,1}\boldsymbol{\xi}_{i,1}^{\mathrm{T}}\boldsymbol{\xi}_{i,1}\Bigg) \\ & - \frac{1}{A_i+b_i}c_{i,1}Q_{i,1} \end{aligned} \tag{28}$$

$$\begin{aligned} \dot{\hat{H}}_{i,1} = & -\frac{3\pi}{2\gamma T_p}\hat{H}_{i,1}^{1+\gamma} - \frac{3\pi}{2\gamma T_p}\hat{H}_{i,1} \\ & + \frac{1}{2p_{i,1}^2}z_{i,1}^2(A_i+b_i)^2\boldsymbol{\xi}_{i,1}^{\mathrm{T}}\boldsymbol{\xi}_{i,1} \end{aligned} \tag{29}$$

where $\chi = \left(\frac{1}{2}\right)^{1+\frac{\gamma}{2}}n^{\frac{\gamma}{2}}$, and $\bar{\chi} = \left(\frac{1}{2}\right)^{1-\frac{\gamma}{2}}$.

Finally, substituting the virtual control law (28) and the adaptive law (29) into (27), the resulting equation is

$$\begin{aligned} \dot{V}_{i,1} \le \sum_{i=1}^{N}\Bigg[ & -\frac{3\pi}{2\gamma T_p}z_{i,1}^{2+\gamma}\chi\tanh\left(\frac{3\pi}{2\gamma T_p}\chi\frac{z_{i,1}^{2+\gamma}}{\mu_{i,1}}\right) \\ & - \frac{3\pi}{2\gamma T_p}z_{i,1}^{2-\gamma}\bar{\chi}\tanh\left(\frac{3\pi}{2\gamma T_p}\bar{\chi}\frac{z_{i,1}^{2-\gamma}}{\mu_{i,1}}\right) \\ & + \frac{3\pi}{2\gamma T_p}\tilde{H}_{i,1}\hat{H}_{i,1}^{1+\gamma} + \frac{3\pi}{2\gamma T_p}\tilde{H}_{i,1}\hat{H}_{i,1} \\ & + z_{i,1}\left(A_i+b_i\right)z_{i,2} + \bar{\Lambda}_{i,1}\Bigg] \end{aligned} \tag{30}$$

where $\bar{\Lambda}_{i,1} = \Lambda_{i,1} + \frac{1}{2}\bar{d}_{i,1}^2 + \frac{1}{2}\bar{d}_{j,1}^2 + \frac{1}{2}\varepsilon_{i,1}^2$.

*Step 2:* Based on the Step 1, the candidate Lyapunov function $V_{i,2}$ is defined as

$$V_{i,2} = V_{i,1} + \sum_{i=1}^{N}\left(\frac{1}{2}z_{i,2}^2 + \frac{1}{2}\tilde{H}_{i,2}^2\right) \tag{31}$$

where $H_{i,2} = \max\left\|\boldsymbol{\Phi}_{i,2}\right\|^2$, $\tilde{H}_{i,2} = H_{i,2} - \hat{H}_{i,2}$, and $\hat{H}_{i,2} \ge 0$ are consistent with the definitions provided in *Step 1*.

The derivative of the error compensation signal is expressed as

$$\begin{aligned} \dot{z}_{i,2} = & z_{i,3} + f_{i,2} + d_{i,2} + \alpha_{i,2} - \dot{\omega}_{i,2} \\ & + \left(A_i+b_i\right)Q_{i,1} + c_{i,2}Q_{i,2} \end{aligned} \tag{32}$$

Differentiating the Lyapunov function yields

$$\begin{aligned} \dot{V}_{i,2} = \dot{V}_{i,1} + \sum_{i=1}^{N}\Bigg[ & z_{i,2}\left(z_{i,3} + f_{i,2} + d_{i,2} + \alpha_{i,2}\right) \\ & + c_{i,2}Q_{i,2} + \left(A_i+b_i\right)Q_{i,1} - z_{i,2}\dot{\omega}_{i,2} \\ & - \tilde{H}_{i,2}\dot{\hat{H}}_{i,2}\Bigg] \end{aligned} \tag{33}$$

Applying Young's inequality leads to

$$z_{i,2}d_{i,2} \leq \frac{1}{2}z_{i,2}^2 + \frac{1}{2}\bar{d}_{i,2}^2 \tag{34}$$

By setting $F_{i,2} = f_{i,2} + (A_i + b_i)\, s_{i,1} + z_{i,2}$ and utilizing *Lemma 9* along with the MTN approximation function, by applying the Young's inequality, we have

$$\begin{aligned} z_{i,2}F_{i,2} &= z_{i,2}\boldsymbol{\Phi}_{i,2}^{\mathrm{T}}\boldsymbol{\xi}_{i,2} + z_{i,2}\delta_{i,2} \\ &\leq \frac{1}{2p_{i,2}^2}z_{i,2}^2 H_{i,2}\boldsymbol{\xi}_{i,2}^{\mathrm{T}}\boldsymbol{\xi}_{i,2} + \Lambda_{i,2} + \frac{1}{2}z_{i,2}^2 \end{aligned} \tag{35}$$

where $p_{i,2} > 0$ is a constant, $\Lambda_{i,2} = \frac{1}{2}p_{i,2}^2 + \frac{1}{2}\varepsilon_{i,2}^2$.

According to (33) and (35), the predefined time virtual control law $\alpha_{i,2}$ and the adaptive law $\dot{\hat{H}}_{i,2}$ are designed as follows

$$\begin{aligned} \alpha_{i,2} = &-\frac{3\pi}{2\gamma T_p}z_{i,2}^{1+\gamma}\chi\tanh\left(\frac{3\pi}{2\gamma T_p}\chi\frac{z_{i,2}^{2+\gamma}}{\mu_{i,2}}\right) \\ &-\frac{3\pi}{2\gamma T_p}z_{i,2}^{1-\gamma}\bar{\chi}\tanh\left(\frac{3\pi}{2\gamma T_p}\bar{\chi}\frac{z_{i,2}^{2-\gamma}}{\mu_{i,2}}\right) \\ &-\frac{1}{2p_{i,2}^2}z_{i,2}\hat{H}_{i,2}\boldsymbol{\xi}_{i,2}^{\mathrm{T}}\boldsymbol{\xi}_{i,2} + \dot{\omega}_{i,2} - c_{i,2}Q_{i,2} \end{aligned} \tag{36}$$

$$\dot{\hat{H}}_{i,2} = -\frac{3\pi}{2\gamma T_p}\hat{H}_{i,2}^{1+\gamma} - \frac{3\pi}{2\gamma T_p}\hat{H}_{i,2} + \frac{1}{2p_{i,2}^2}z_{i,2}^2\boldsymbol{\xi}_{i,2}^{\mathrm{T}}\boldsymbol{\xi}_{i,2} \tag{37}$$

Substituting the virtual control law (36) and adaptive law (37) into (35) results in

$$\begin{aligned} \dot{V}_{i,2} \leq \sum_{i=1}^{N}\Bigg[ &-\sum_{r=1}^{2}\frac{3\pi}{2\gamma T_p}z_{i,r}^{2+\gamma}\chi\tanh\left(\frac{3\pi}{2\gamma T_p}\chi\frac{z_{i,r}^{2+\gamma}}{\mu_{i,r}}\right) \\ &-\sum_{r=1}^{2}\frac{3\pi}{2\gamma T_p}z_{i,r}^{2-\gamma}\bar{\chi}\tanh\left(\frac{3\pi}{2\gamma T_p}\bar{\chi}\frac{z_{i,r}^{2-\gamma}}{\mu_{i,r}}\right) \\ &+\sum_{r=1}^{2}\frac{3\pi}{2\gamma T_p}\tilde{H}_{i,r}\hat{H}_{i,r}^{1+\gamma} + \sum_{r=1}^{2}\frac{3\pi}{2\gamma T_p}\tilde{H}_{i,r}\hat{H}_{i,r} \\ &+ z_{i,2}z_{i,3} + \bar{\Lambda}_{i,2}\Bigg] \end{aligned} \tag{38}$$

where $\bar{\Lambda}_{i,2} = \Lambda_{i,2} + \frac{1}{2}\bar{d}_{i,r}^2 + \bar{\Lambda}_{i,1}$.

*Step j*$(j = 3, \ldots, n-1)$: Considering the following Lyapunov function $V_{i,j}$ as

$$V_{i,j} = V_{i,j-1} + \sum_{i=1}^{N}\left(\frac{1}{2}z_{i,j}^2 + \frac{1}{2}\tilde{H}_{i,j}^2\right) \tag{39}$$

where $H_{i,j} = \max\left\|\boldsymbol{\Phi}_{i,j}\right\|^2$, $\tilde{H}_{i,j} = H_{i,j} - \hat{H}_{i,j}$, and $\hat{H}_{i,j} \geq 0$ are consistent with the definitions provided in *Step 1*.

Differentiating the Lyapunov function yields

$$\begin{aligned} \dot{V}_{i,j} = \dot{V}_{i,j} + \sum_{i=1}^{N}\Bigg[ &z_{i,j}\left(z_{i,j+1} + f_{i,j} + d_{i,j} + \alpha_{i,j}\right) \\ &+ Q_{i,j-1} + c_{i,j}Q_{i,j} - z_{i,j}\dot{\omega}_{i,j} - \tilde{H}_{i,j}\dot{\hat{H}}_{i,j}\Bigg] \end{aligned} \tag{40}$$

Applying Young's inequality leads to

$$z_{i,j}d_{i,j} \leq \frac{1}{2}z_{i,j}^2 + \frac{1}{2}\bar{d}_{i,j}^2 \tag{41}$$

By setting $F_{i,j} = f_{i,j} + s_{i,j-1} + z_{i,j}$ and utilizing *Lemma 9* along with the MTN approximation function, by applying the Young's inequality, we have

$$\begin{aligned} z_{i,j}F_{i,j} &= z_{i,j}\boldsymbol{\Phi}_{i,j}^{\mathrm{T}}\boldsymbol{\xi}_{i,j} + z_{i,j}\delta_{i,j} \\ &\leq \frac{1}{2p_{i,j}^2}z_{i,j}^2 H_{i,j}\boldsymbol{\xi}_{i,j}^{\mathrm{T}}\boldsymbol{\xi}_{i,j} + \Lambda_{i,j} + \frac{1}{2}z_{i,j}^2 \end{aligned} \tag{42}$$

where $p_{i,j} > 0$ is a constant, $\Lambda_{i,j} = \frac{1}{2}p_{i,j}^2 + \frac{1}{2}\varepsilon_{i,j}^2$.

According to (40) and (42), the predefined time virtual control law $\alpha_{i,j}$ and the adaptive law $\dot{\hat{H}}_{i,j}$ are designed as follows

$$\begin{aligned} \alpha_{i,j} = &-\frac{3\pi}{2\gamma T_p}z_{i,j}^{1+\gamma}\chi\tanh\left(\frac{3\pi}{2\gamma T_p}\chi\frac{z_{i,j}^{2+\gamma}}{\mu_{i,j}}\right) \\ &\times\frac{3\pi}{2\gamma T_p}z_{i,j}^{1-\gamma}\bar{\chi}\tanh\left(\frac{3\pi}{2\gamma T_p}\bar{\chi}\frac{z_{i,j}^{2-\gamma}}{\mu_{i,j}}\right) \\ &-\frac{1}{2p_{i,j}^2}z_{i,j}\hat{H}_{i,j}\boldsymbol{\xi}_{i,j}^{\mathrm{T}}\boldsymbol{\xi}_{i,j} + \dot{\omega}_{i,j} - c_{i,j}Q_{i,j} \end{aligned} \tag{43}$$

$$\dot{\hat{H}}_{i,j} = -\frac{3\pi}{2\gamma T_p}\hat{H}_{i,j}^{1+\gamma} - \frac{3\pi}{2\gamma T_p}\hat{H}_{i,j} + \frac{1}{2p_{i,j}^2}z_{i,j}^2\boldsymbol{\xi}_{i,j}^{\mathrm{T}}\boldsymbol{\xi}_{i,j} \tag{44}$$

Substituting the virtual control law (43) and adaptive law (44) into (42) results in

$$\begin{aligned}\dot{V}_{i,j} \leq \sum_{i=1}^{N}\Bigg[ &-\sum_{r=1}^{j}\frac{3\pi}{2\gamma T_p}z_{i,r}^{2+\gamma}\chi\tanh\left(\frac{3\pi}{2\gamma T_p}\chi\frac{z_{i,r}^{2+\gamma}}{\mu_{i,r}}\right)\\ &-\sum_{r=1}^{j}\frac{3\pi}{2\gamma T_p}z_{i,r}^{2-\gamma}\bar{\chi}\tanh\left(\frac{3\pi}{2\gamma T_p}\bar{\chi}\frac{z_{i,r}^{2-\gamma}}{\mu_{i,r}}\right)\\ &+\sum_{r=1}^{j}\frac{3\pi}{2\gamma T_p}\tilde{H}_{i,r}\hat{H}_{i,r}^{1+\gamma}+\sum_{r=1}^{j}\frac{3\pi}{2\gamma T_p}\tilde{H}_{i,r}\hat{H}_{i,r}\\ &+z_{i,j}z_{i,j+1}+\bar{\Lambda}_{i,j}\Bigg]\end{aligned} \tag{45}$$

where $\bar{\Lambda}_{i,j}=\Lambda_{i,j}+\frac{1}{2}\bar{d}_{i,j}^2+\bar{\Lambda}_{i,j-1}$.

*Step n:* Choosing the candidate Lyapunov function as

$$V_{i,n}=V_{i,n-1}+\sum_{i=1}^{N}\left(\frac{1}{2k_{i1}}z_{i,n}^2+\frac{1}{2}\tilde{H}_{i,n}^2\right) \tag{46}$$

where $H_{i,n}=\max\left\|\boldsymbol{\Phi}_{i,n}\right\|^2$, $\tilde{H}_{i,n}=H_{i,n}-\hat{H}_{i,n}$, $\hat{H}_{i,n}\geq 0$. $k_{i1}>0$ is a constant.

The derivative of the error compensation signal $z_{i,n}$ is given by

$$\begin{aligned}\dot{z}_{i,n}=&h_iu_i+f_{i,n}+d_{i,n}-\dot{\omega}_{i,n}\\ &+k_{i1}c_{i,n}Q_{i,n}+k_{i1}Q_{i,n-1}\end{aligned} \tag{47}$$

Taking the derivative of the Lyapunov function yields

$$\begin{aligned}\dot{V}_{i,n}=\dot{V}_{i,n-1}+\sum_{i=1}^{N}\Bigg[&\frac{1}{k_{i1}}z_{i,n}\left(h_{i,n}u_i+f_{i,n}+d_{i,n}-\dot{\omega}_{i,n}\right)\\ &+z_{i,n}c_{i,n}Q_{i,n}+z_{i,n}s_{i,n-1}-z_{i,n}z_{i,n-1}-\tilde{H}_{i,n}\dot{\hat{H}}_{i,n}\Bigg]\end{aligned} \tag{48}$$

From the input saturation model presented in *Lemma 8*, it follows that

$$u_i\left(v_i\left(t\right)\right)=\rho_i\left(v_i\left(t\right)\right)+\delta_i\left(v_i(t)\right) \tag{49}$$

Combining (48) and (49), $\dot{V}_{i,n}$ can be reformulated as

$$\begin{aligned}\dot{V}_{i,n}=\dot{V}_{i,n-1}+\sum_{i=1}^{N}\Bigg[&\frac{1}{k_{i1}}z_{i,n}\left(h_{i,n}\rho_i\left(v_i\left(t\right)\right)+h_i\delta_i+f_{i,n}\right)\\ &+\frac{1}{k_{i1}}z_{i,n}\left(d_{i,n}-\dot{\omega}_{i,n}\right)+z_{i,n}c_{i,n}Q_{i,n}+z_{i,n}s_{i,n-1}\\ &-z_{i,n}z_{i,n-1}-\tilde{H}_{i,n}\dot{\hat{H}}_{i,n}\Bigg]\end{aligned} \tag{50}$$

By applying Young's inequality and *Lemma 7*, we derive

$$\frac{1}{k_{i1}}z_{i,n}d_{i,n}\leq\frac{1}{2k_{i1}^2}z_{i,n}^2+\frac{1}{2}\bar{d}_{i,n}^2 \tag{51}$$

$$\frac{1}{k_{i1}}z_{i,n}h_i\delta_i\leq\frac{1}{k_{i1}}z_{i,n}a_{i,M}M_i\leq\frac{a_{i,M}^2}{2k_{i1}^2}z_{i,n}^2+\frac{1}{2}M_i^2 \tag{52}$$

Choosing $F_{i,n}=\frac{1}{k_{i1}}f_{i,n}+s_{i,n-1}+\left(\frac{1}{2}+\frac{1}{2k_{i1}^2}+\frac{a_{i,M}^2}{2k_{i1}^2}\right)z_{i,n}$, and using *Lemma 9* and the MTN approximation function, along with Young's inequality, we obtain

$$\begin{aligned}z_{i,n}F_{i,n}&=z_{i,n}\boldsymbol{\Phi}_{i,n}^{\mathrm{T}}\boldsymbol{\xi}_{i,n}+z_{i,n}\delta_{i,n}\\ &\leq\frac{1}{2p_{i,n}^2}z_{i,n}^2H_{i,n}\boldsymbol{\xi}_{i,n}^{\mathrm{T}}\boldsymbol{\xi}_{i,n}+\Lambda_{i,n}+\frac{1}{2}z_{i,n}^2\end{aligned} \tag{53}$$

where $p_{i,n}>0$ is a constant, $\Lambda_{i,n}=\frac{1}{2}p_{i,n}^2+\frac{1}{2}\varepsilon_{i,n}^2$.

Substituting (51), (52), and (53) into (50) results in

$$\begin{aligned}\dot{V}_{i,n}\leq\dot{V}_{i,n-1}+\sum_{i=1}^{N}\Bigg[&\frac{1}{k_{i1}}z_{i,n}h_{i,n}\rho_i\left(v_i\left(t\right)\right)-\frac{1}{k_{i1}}z_{i,n}\dot{\omega}_{i,n}\\ &+z_{i,n}c_{i,n}Q_{i,n}+\frac{1}{2p_{i,n}^2}z_{i,n}^2H_{i,n}\boldsymbol{\xi}_{i,n}^{\mathrm{T}}\boldsymbol{\xi}_{i,n}\\ &+\Lambda_{i,n}+\frac{1}{2}M_i^2+\frac{1}{2}\bar{d}_{i,n}^2\Bigg]\end{aligned} \tag{54}$$

Similarly to step $j$, we define the virtual control function $\varphi_i\left(z_{i,n},\boldsymbol{\xi}_{i,n}\right)$ as

$$\varphi_i\left(z_{i,n},\boldsymbol{\xi}_{i,n}\right)=-\frac{3\pi}{2\gamma T_p}z_{i,n}^{1+\gamma}\chi\tanh\left(\frac{3\pi}{2\gamma T_p}\chi\frac{z_{i,n}^{2+\gamma}}{\mu_{i,n}}\right)-\frac{3\pi}{2\gamma T_p}z_{i,n}^{1-\gamma}\bar{\chi}\tanh\left(\frac{3\pi}{2\gamma T_p}\bar{\chi}\frac{z_{i,n}^{2-\gamma}}{\mu_{i,n}}\right)-\frac{1}{2p_{i,n}^2}z_{i,n}\hat{H}_{i,n}\boldsymbol{\xi}_{i,n}^{\mathrm{T}}\boldsymbol{\xi}_{i,n}+\frac{1}{k_{i1}}\dot{\omega}_{i,n}-z_{i,n-1}-c_{i,n}Q_{i,n} \tag{55}$$

Accordingly, the smooth function $\rho_i\left(v_i\left(t\right)\right)$ is designed as

$$\rho_i\left(v_i\left(t\right)\right)=k_{i1}a_{im}^{-1}\varphi_i\left(z_{i,n},\boldsymbol{\xi}_{i,n}\right) \tag{56}$$

The adaptive law $\dot{\hat{H}}_{i,n}$ is determined as

$$\dot{\hat{H}}_{i,n}=-\frac{3\pi}{2\gamma T_p}\hat{H}_{i,n}^{1+\gamma}-\frac{3\pi}{2\gamma T_p}\hat{H}_{i,n}+\frac{1}{2p_{i,n}^2}z_{i,n}^2\boldsymbol{\xi}_{i,n}^{\mathrm{T}}\boldsymbol{\xi}_{i,n} \tag{57}$$

By substituting $\rho_i\left(v_i\left(t\right)\right)$ and the adaptive law (57) into the equations, we achieve

$$\dot{V}_{i,n}\le\sum_{i=1}^{N}\Bigg[-\sum_{r=1}^{n}\frac{3\pi}{2\gamma T_p}z_{i,r}^{2+\gamma}\chi\tanh\left(\frac{3\pi}{2\gamma T_p}\chi\frac{z_{i,r}^{2+\gamma}}{\mu_{i,r}}\right)-\sum_{r=1}^{n}\frac{3\pi}{2\gamma T_p}z_{i,r}^{2-\gamma}\bar{\chi}\tanh\left(\frac{3\pi}{2\gamma T_p}\bar{\chi}\frac{z_{i,r}^{2-\gamma}}{\mu_{i,r}}\right)+\sum_{r=1}^{n}\frac{3\pi}{2\gamma T_p}\tilde{H}_{i,r}\hat{H}_{i,r}+\sum_{r=1}^{n}\frac{3\pi}{2\gamma T_p}\tilde{H}_{i,r}\hat{H}_{i,r}^{1+\gamma}+\bar{\Lambda}_{i,n}\Bigg] \tag{58}$$

where $\bar{\Lambda}_{i,n}=\Lambda_{i,n}+\frac{1}{2}\bar{d}_{i,n}^2+\frac{1}{2}M_i^2+\bar{\Lambda}_{i,n-1}$.

**Controller Design:** Consider a nonlinear multi-agent system with input saturation $u_i(v_i(t),k_i)$. To ensure the solvability of the equations $\rho_i\left(v_i\left(t\right)\right)=k_{i1}a_{im}^{-1}\varphi_i\left(s_{i,n},\boldsymbol{\xi}_{i,n}\right)$, the controller $v_i(t)$ can be designed by solving the given equations. From $u_i\left(v_i\left(t\right)\right)=\rho_i\left(v_i\left(t\right)\right)+\delta_i\left(v_i(t)\right)$ and *Lemma 8*, the following is derived

$$\rho_i\left(v_i\left(t\right)\right)=k_{i1}u_{im}(v_i(t)) \tag{59}$$

Since $u_{im}(v_i(t))$ is injective, the controller is expressed as

$$\dot{\hat{H}}_{i,n}=-\frac{3\pi}{2\gamma T_p}\hat{H}_{i,n}^{1+\gamma}-\frac{3\pi}{2\gamma T_p}\hat{H}_{i,n}+\frac{1}{2p_{i,n}^2}z_{i,n}^2\boldsymbol{\xi}_{i,n}^{\mathrm{T}}\boldsymbol{\xi}_{i,n} \tag{60}$$

Based on (60), the final form of the designed controller is

$$v_i(t)=\begin{cases}r_a+\dfrac{\varphi-a_{im}r_a}{a_{im}-a_{im}r_a+\varphi}, & a_{im}(r_a-1)<\varphi<a_{im}r_a\\ \dfrac{\varphi}{a_{im}}, & a_{im}r_a\le\varphi\le a_{im}r_b\\ r_b+\dfrac{\varphi-a_{im}r_b}{a_{im}+a_{im}r_b-\varphi}, & a_{im}r_b<\varphi<a_{im}(r_b+1)\end{cases} \tag{61}$$

### 3.3 Stability analysis

**Theorem 1** *Consider a strict-feedback nonlinear multi-agent system* (1) *with input saturation* (12)*. By designing command filters* (18)*, virtual control laws* (28)*,* (36)*,* (43)*,* (55)*, controllers* (61)*, and adaptive laws* (29)*,* (37)*,* (44)*,* (57)*, it can be shown that the system achieves practical predefined time stability. Additionally, the tracking error converges to a small neighborhood around the origin within the predefined time.*

*Proof* Based on *Lemma 3*, there exist constants $\mu_{i,r}>0$, and $k=0.2785$ such that the following inequalities hold

$$-\frac{3\pi}{2\gamma T_p}z_{i,r}^{2+\gamma}\chi\tanh\left(\frac{3\pi}{2\gamma T_p}\chi\frac{z_{i,r}^{2+\gamma}}{\mu_{i,r}}\right)\le-\frac{3\pi}{2\gamma T_p}\chi z_{i,r}^{2+\gamma}+k\mu_{i,r} \tag{62}$$

$$-\frac{3\pi}{2\gamma T_p}z_{i,r}^{2-\gamma}\bar{\chi}\tanh\left(\frac{3\pi}{2\gamma T_p}\bar{\chi}\frac{z_{i,r}^{2-\gamma}}{\mu_{i,r}}\right)\le-\frac{3\pi}{2\gamma T_p}\bar{\chi}z_{i,r}^{2-\gamma}+k\mu_{i,r} \tag{63}$$

□

Substituting (62) and (63) into (58) yields

$$\begin{aligned}\dot{V}_{i,n} \leq & -\sum_{r=1}^{n}\frac{3\pi}{2\gamma T_p}\chi z_{i,r}^{2+\gamma} - \sum_{r=1}^{n}\frac{3\pi}{2\gamma T_p}\bar{\chi} z_{i,r}^{2-\gamma} \\ & + \sum_{r=1}^{n}\frac{3\pi}{2\gamma T_p}\tilde{H}_{i,r}\hat{H}_{i,r} \\ & + \sum_{r=1}^{n}\frac{3\pi}{2\gamma T_p}\tilde{H}_{i,r}\hat{H}_{i,r}^{1+\gamma} + \Omega_{i,n}\end{aligned} \tag{64}$$

where $\Omega_{i,n} = \bar{\Lambda}_{i,n} + 2nk\mu_{i,r}$.

By applying *Lemma 4*, the following results can be obtained

$$-\sum_{r=1}^{n}\frac{3\pi}{2\gamma T_p}\chi z_{i,r}^{2+\gamma} \leq -\frac{3\pi}{2\gamma T_p}\left(\sum_{r=1}^{n}\frac{1}{2}z_{i,r}^{2}\right)^{1+\frac{\gamma}{2}} \tag{65}$$

$$-\sum_{r=1}^{n}\frac{3\pi}{2\gamma T_p}\bar{\chi} z_{i,r}^{2-\gamma} \leq -\frac{3\pi}{2\gamma T_p}\left(\sum_{r=1}^{n}\frac{1}{2}z_{i,r}^{2}\right)^{1-\frac{\gamma}{2}} \tag{66}$$

Using Young's inequality, it follows that

$$\frac{3\pi}{2\gamma T_p}\tilde{H}_{i,r}\hat{H}_{i,r} \leq \frac{3\pi}{2\gamma T_p}\left(-\frac{1}{2}\tilde{H}_{i,r}^{2} + \frac{1}{2}H_{i,r}^{2}\right) \tag{67}$$

Furthermore, invoking *Lemma 5* provides

$$\begin{aligned}-\frac{3\pi}{2\gamma T_p}\left(\frac{1}{2}\tilde{H}_{i,r}^{2}\right) \leq & \frac{3\pi}{2\gamma T_p}\frac{\gamma}{2}\left(\frac{2-\gamma}{2}\right)^{\frac{2-\gamma}{\gamma}} \\ & - \frac{3\pi}{2\gamma T_p}\left(\frac{1}{2}\tilde{H}_{i,r}^{2}\right)^{1-\frac{\gamma}{2}}\end{aligned} \tag{68}$$

Combining *Lemma 4* with (68) leads to

$$-\sum_{r=1}^{n}\frac{3\pi}{2\gamma T_p}\left(\frac{1}{2}\tilde{H}_{i,r}^{2}\right)^{1-\frac{\gamma}{2}} \leq -\frac{3\pi}{2\gamma T_p}\left(\sum_{r=1}^{n}\frac{1}{2}\tilde{H}_{i,r}^{2}\right)^{1-\frac{\gamma}{2}} \tag{69}$$

From *Lemma 6*, the following inequality is derived

$$\begin{aligned}\frac{3\pi}{2\gamma T_p}\tilde{H}_{i,r}\hat{H}_{i,r}^{1+\gamma} &\leq \frac{3\pi}{2\gamma T_p}\tilde{H}_{i,r}\left(H_{i,r} - \tilde{H}_{i,r}\right)^{1+\gamma} \\ &\leq \frac{3\pi}{2\gamma T_p}\frac{1+\gamma}{2+\gamma}\left(H_{i,r}^{2+\gamma} - \tilde{H}_{i,r}^{2+\gamma}\right) \\ &\leq \frac{3\pi}{2\gamma T_p}\frac{1+\gamma}{2+\gamma}H_{i,r}^{2+\gamma} - \frac{3\pi}{2\gamma T_p}\left(\frac{1}{2}\tilde{H}_{i,r}^{2}\right)^{1+\frac{\gamma}{2}}\end{aligned} \tag{70}$$

Substituting (65), (66), (67), (68), (69), and (70) into (64) yields the final relationship

$$\dot{V}_{i,n} \leq -\frac{3\pi}{2\gamma T_p}\left(V_{i,n}^{1+\frac{\gamma}{2}} + V_{i,n}^{1-\frac{\gamma}{2}}\right) + \sigma_{i,n} \tag{71}$$

where $\sigma_{i,n} = \frac{3\pi}{2\gamma T_p}\frac{1+\gamma}{2+\gamma}H_{i,r}^{2+\gamma} + \frac{3\pi}{2\gamma T_p}\frac{1}{2}H_{i,r}^{2} + \frac{3\pi}{2\gamma T_p}\frac{\gamma}{2}\left(\frac{2-\gamma}{2}\right)^{\frac{2-\gamma}{\gamma}} + \Omega_{i,n}$. According to *Lemma 2*, it can be concluded that as $t \geq T_p$, the system's tracking error converges to a small neighborhood around the origin, and $V_{i,n}$ satisfying $\left\{V_{i,n} \leq \frac{2\gamma T_p \sigma}{3\pi}\right\}$. Due to the properties of the Lyapunov function designed in this study, the error compensation signals $z_{i,j}$ and estimation errors $\tilde{H}_{i,j}$ are bounded, ensuring that all related variables remain bounded. Based on this analysis, it can be concluded that all signals in the closed-loop system are bounded. Thus, the proof of the theorem is complete.

*Remark 5* The predefined time control method proposed in this paper ensures that the synchronization error in MASs converge to a small neighborhood around the origin within a predetermined time, thus guaranteeing that the system reaches its desired state in a timely manner. This method is particularly suitable for systems that require rapid convergence and where synchronization accuracy is critical, such as in scenarios with minimal disturbances and well-structured system dynamics. However, it is important to note that although the method effectively handles synchronization under ideal conditions, its direct application to practical systems with physical constraints (e.g., drone systems or autonomous vehicles) may present challenges. Specifically, as the synchronization error $e_i$ converges to a very small neighborhood, the agents may become too close to each other, potentially resulting in conflicts.

## 4 Simulation results

In this section, the effectiveness and practicality of the proposed control scheme are demonstrated through two simulation examples. The communication topology is shown in Fig. 2, from which the Laplacian matrix is derived as follows $\mathcal{L} = \begin{pmatrix} 0 & 0 & 0 & 0 \\ -1 & 1 & 0 & 0 \\ 0 & -1 & 1 & 0 \\ -1 & 0 & 0 & 1 \end{pmatrix}$.

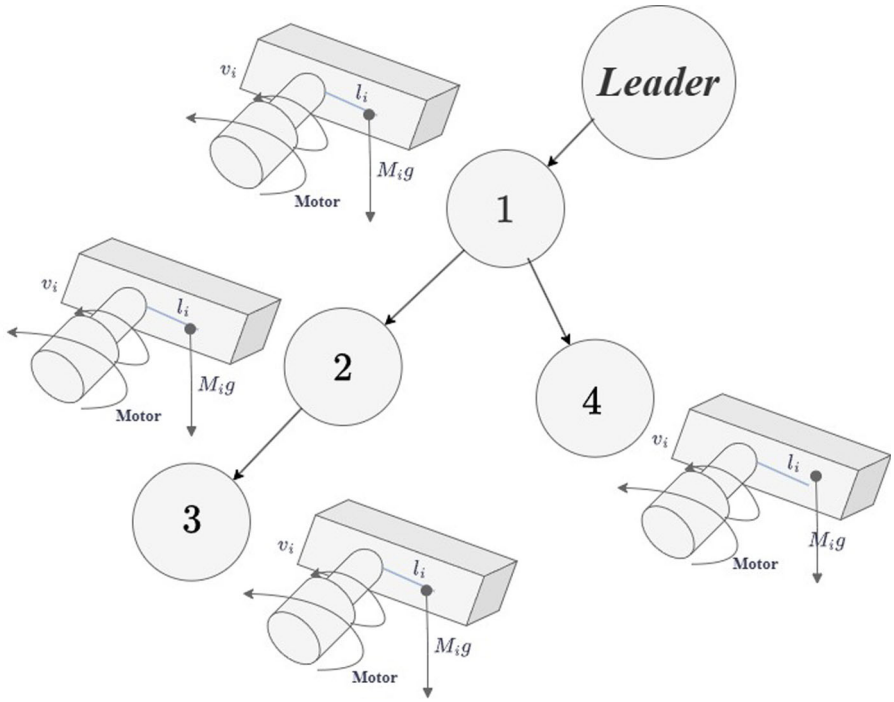


**Fig. 2** Communication topology

### 4.1 Numerical example

Consider a nonlinear multi-agent system with one leader and four followers. The dynamics of the $i$ -th follower are described as follows

$$\begin{cases} \dot{x}_{i,1} = x_{i,2} - 0.5x_{i,1} \\ \dot{x}_{i,2} = u_i(v_i(t)) + 0.1x_{i,2}e^{x_{i,1}} + d_i(t) \\ y_i = x_{i,1} \end{cases} \tag{72}$$

where $u_i \in \Re$ and $y_i \in \Re$ represent the input and output of each agent, respectively, $d_i(t)$ denotes external disturbances. The saturation function is applied to $u_i(v_i(t))$.
The external disturbance is given as

$$d_i(t) = 0.1\sin(t) \tag{73}$$

The leader's reference signal is

$$y_d = \sin(t) \tag{74}$$

According to (12), each agent is assigned a distinct asymmetric input saturation limit. Specifically, the input saturation limits for agent 1, agent 2, agent 3, and agent 4 are set to $u_1 \in [-6, 20]$, $u_2 \in [-3, 10]$, $u_3 \in [-5, 15]$, and $u_4 \in [-4, 12]$, respectively.

Parameters are chosen as $T_p = 5\,s$, $\gamma = 0.2$, $\upsilon_{1,2} = 100$, $\upsilon_{2,2} = 100$, $\upsilon_{3,2} = 100$,$\upsilon_{4,2} = 10$, $c_{1,1} = 20$, $c_{1,2} = c_{2,2} = c_{3,2} = c_{4,2} = 1$, $c_{2,1} = c_{3,1} = c_{4,1} = 10$, $\varepsilon_{1,1} = \varepsilon_{1,2} = 0.01$, $\varepsilon_{1,3} = 0.1$, $\varepsilon_{1,4} = 0.001$, $p_{1,1} = 0.0005$, $p_{1,2} = p_{2,2} = p_{3,2} = p_{4,2} = 1$, $p_{2,1} = p_{3,1} = 0.002$, $p_{4,1} = 0.001$, $k_{1,1} = k_{2,1} = k_{3,1} = k_{4,1} = 1$, $r_a = -30$, $r_b = 20$, $a_{1\,m} = a_{2\,m} = a_{3\,m} = a_{4\,m} = 2$. The initial values of all agent systems are set to $\bar{x}_{1,2}(0) = \left[x_{1,1}(0), x_{1,2}(0)\right] = [0.05, 0.2]^{\mathrm{T}}$, $\bar{x}_{2,2}(0) = \left[x_{2,1}(0), x_{2,2}(0)\right] = [0.02, 0.1]^{\mathrm{T}}$, $\bar{x}_{3,2}(0) = \left[x_{3,1}(0), x_{3,2}(0)\right] = [0.01, 0.2]^{\mathrm{T}}$, $\bar{x}_{4,2}(0) = \left[x_{3,1}(0), x_{3,2}(0)\right] = [0.02, 0.1]^{\mathrm{T}}$.

Simulation results are shown in Figs. 3, 4, 5 and 6. Figures 3 and 4 illustrate the tracking error and its convergence behavior. It can be observed that the proposed predefined time control strategy ensures that the tracking error converges to a small neighborhood of the origin within the predefined time, verifying the rapid convergence performance of the control system. Figures 5 and 6 compare the variations of the virtual control input and the actual control input under saturation conditions, demonstrating that the designed control law remains effective even when each agent is subjected to differ-

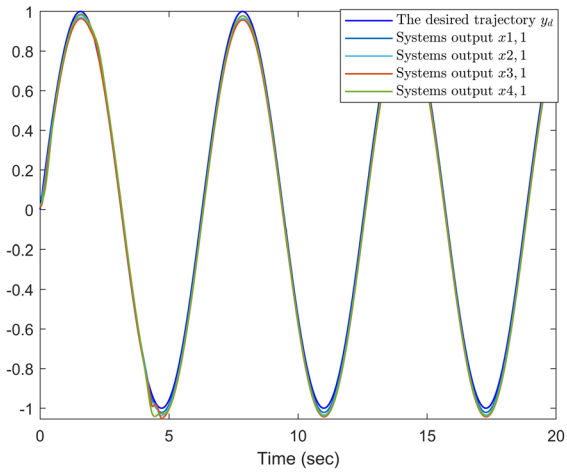


**Fig. 3** Leader-follower tracking signals

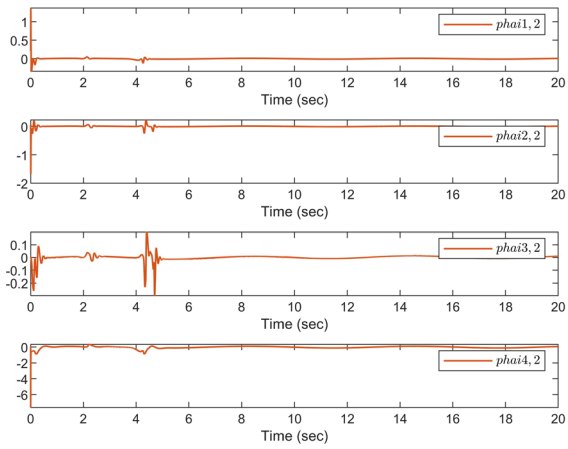


**Fig. 4** Filtering error

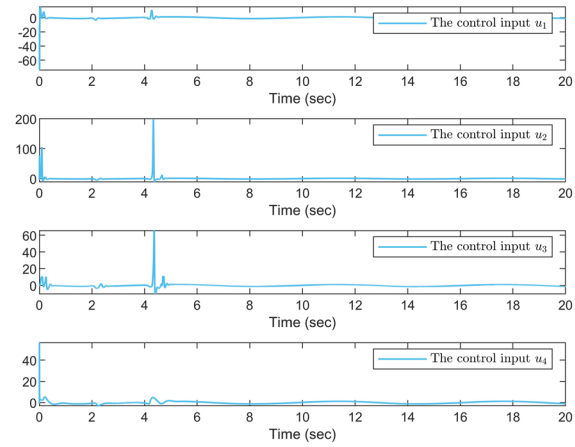


**Fig. 5** Designed virtual control input

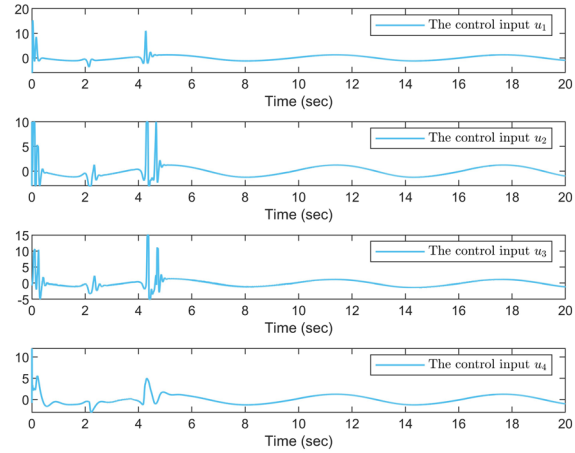


**Fig. 6** Actual control input under saturation

ent input saturation constraints, thereby ensuring the system's control performance.

## 4.2 Practical example

To further validate the proposed control strategy, a multi-agent system consisting of four single-link robotic arms is considered, with a communication topology as shown in Fig. 2.

The dynamics of the $i$-th follower are described as

$$\begin{cases} \dot{v}_i = q_i \\ M_i \ddot{q}_i + km_i g l_i \sin(q_i) = u_i(v_i(t)) + d_i(t) \end{cases} \tag{75}$$

where $i = 1, 2, 3, 4$, parameter is chosen as $k = 0.5$. $M = 1\,kg * m^2$ represents the moment of inertia, $m_i = 1\,kg$ and $l_i = 1m$ denote the mass and length of the arm, $g = 9.8m/s^2$ is the gravitational constant, $q_i$, $\dot{q}_i$, and $\ddot{q}_i$ are the angular position, velocity, and acceleration, respectively. The input $u_i(v_i(t))$ is subject to a saturation function, and $d_i(t)$ represents external disturbances. The external disturbance is modeled as

$$d_i(t) = 0.5 \sin(t) \tag{76}$$

The leader's reference signal is

$$y_d = \sin(t) \tag{77}$$

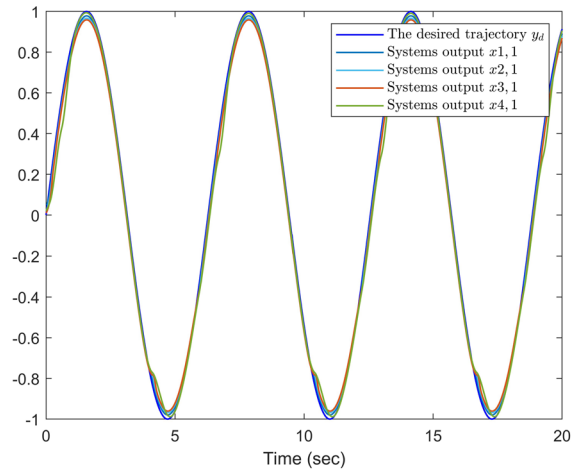


**Fig. 7** Leader-follower tracking signals

The asymmetric input saturation is given by

$$u_i(v_i(t)) = \begin{cases} 30, & u_i > 30 \\ u_i, & -15 \le u_i \le 30 \\ -15, & u_i < -15 \end{cases} \tag{78}$$

Parameters are chosen as $T_p = 5\,s$, $\gamma = 0.2$, $\upsilon_{1,2} = 100$, $\upsilon_{2,2} = 100$, $\upsilon_{3,2} = 100$,$\upsilon_{4,2} = 10$, $c_{1,1} = 20$, $c_{1,2} = c_{2,2} = c_{3,2} = c_{4,2} = 1$, $c_{2,1} = c_{3,1} = c_{4,1} = 10$, $c_{4,1} = 5$, $\varepsilon_{1,1} = \varepsilon_{1,2} = 0.01$, $\varepsilon_{1,3} = 0.1$, $\varepsilon_{1,4} = 0.001$, $p_{1,1} = 0.0005$, $p_{1,2} = p_{2,2} = p_{3,2} = p_{4,2} = 1$, $p_{2,1} = 0.002$, $p_{3,1} = 0.0001$, $p_{4,1} = 0.001$, $k_{1,1} = k_{2,1} = k_{3,1} = k_{4,1} = 1$, $r_a = -30$, $r_b = 20$, $a_{1\,m} = a_{2\,m} = a_{3\,m} = a_{4\,m} = 2$. The initial values of all agent systems are set to $\bar{x}_{1,2}(0) = \left[x_{1,1}(0), x_{1,2}(0)\right] = [0.05, 0.2]^{\mathrm{T}}$, $\bar{x}_{2,2}(0) = \left[x_{2,1}(0), x_{2,2}(0)\right] = [0.02, 0.1]^{\mathrm{T}}$, $\bar{x}_{3,2}(0) = \left[x_{3,1}(0), x_{3,2}(0)\right] = [0.01, 0.2]^{\mathrm{T}}$, $\bar{x}_{4,2}(0) = \left[x_{3,1}(0), x_{3,2}(0)\right] = [0.02, 0.1]^{\mathrm{T}}$.

Simulation results are illustrated in Figs. 7, 8, 9 and 10. Figures 7 and 8 demonstrate that under the selected parameters and controller design, all followers achieve precise tracking of the leader's reference signal within the predefined time, confirming the high-accuracy control of the proposed strategy. Figures 9 and 10 indicate that while the control input demand is relatively high for maintaining system stability, the designed saturation approximation function significantly reduces the required input, thus minimizing control energy consumption.

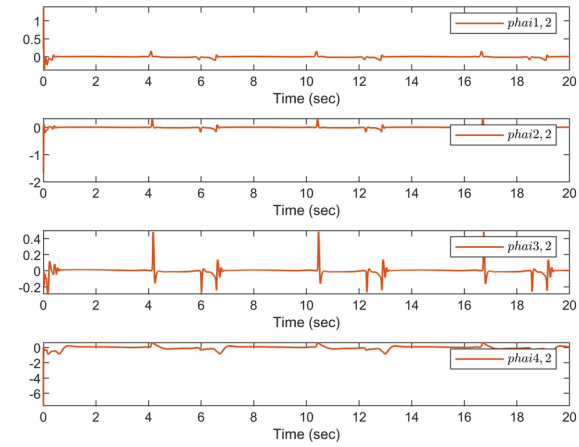


**Fig. 8** Filtering error

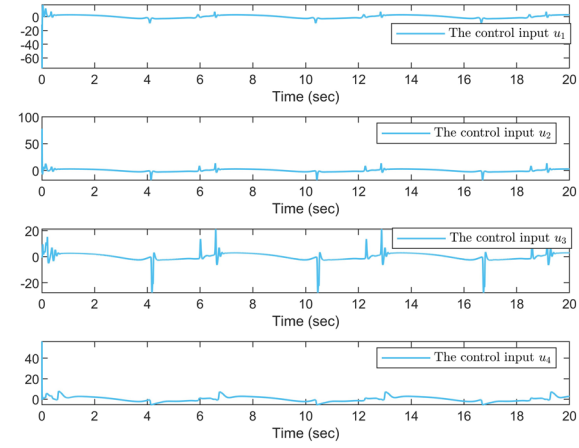


**Fig. 9** Designed virtual control input

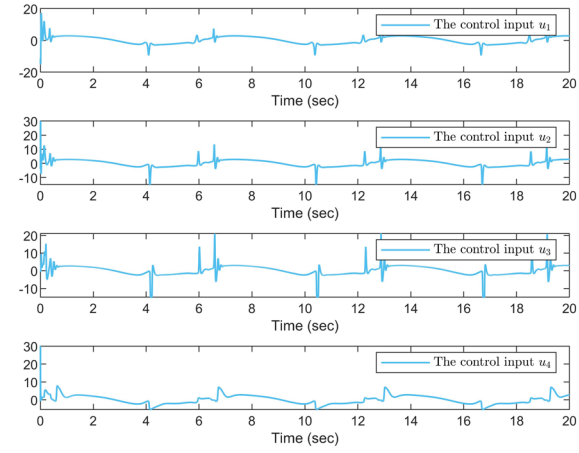


**Fig. 10** Actual control input under saturation

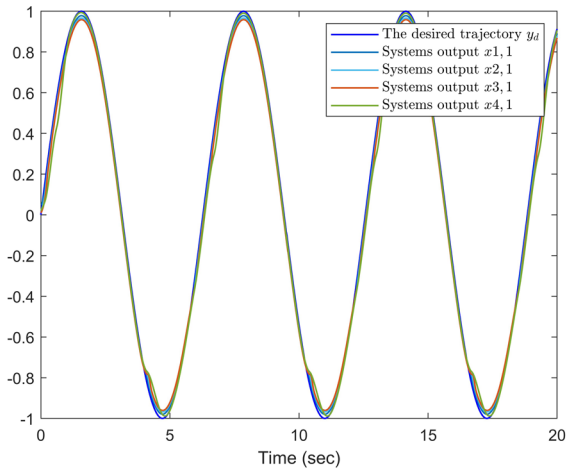


(a) Tracking curve of the proposed method

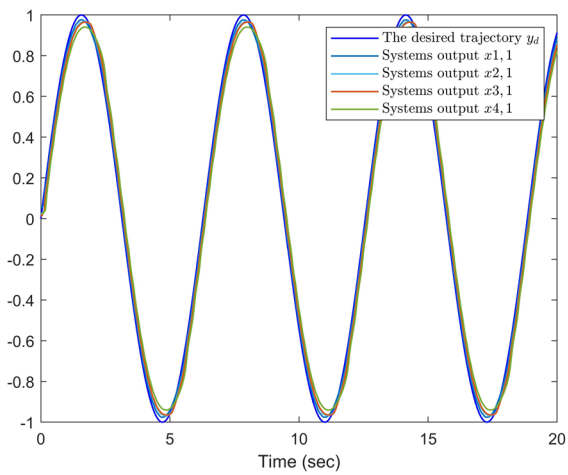


(b) Tracking curve of conventional predefined time control

**Fig. 11** Comparison of Tracking Curves

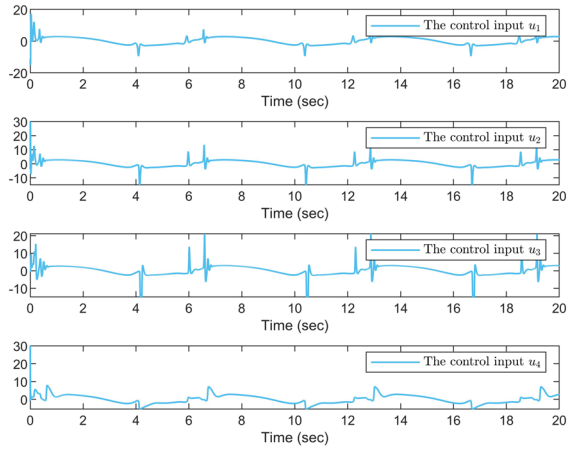


(a) Control input of the proposed method

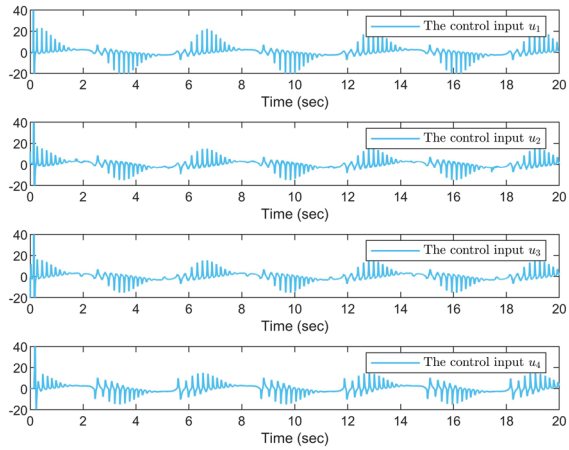


(b) Control input of conventional predefined time control

**Fig. 12** Comparison of control input

## 4.3 Comparative experiments

To highlight the advantages of the proposed control scheme, we conducted the following comparative experiments.

(1)We compare the predefined time control method introduced in this paper with conventional predefined time control to evaluate tracking performance and control chattering. By selecting identical settling time $T_P = 1s$ and predefined time parameters $\gamma = 0.2$, the remaining conditions are the same as those in the actual example.

Simulation results are shown as follows. Figure 11a presents the tracking curve for the proposed method, Fig. 11b shows the tracking curve for conventional predefined time control, Fig. 12a displays the control input for the proposed method, and Fig. 12b illustrates the control input for conventional predefined time control. As depicted in Figs. 11 and 12, although the approach utilizing a sign function to handle the singularity inherent in predefined time control yields similar tracking performance, a comparison of the control inputs reveals that the controller based on the traditional sign function induces substantial chattering in the control input. In contrast, the control input generated by the predefined time filter, which employs a hyperbolic tangent function, effectively alleviates such chattering.

(2)To validate the advantages of the proposed control scheme over finite-time control, we conduct a

comparative experiment by selecting larger initial conditions. The initial conditions are set as $\bar{x}_{1,2}(0) = \left[x_{1,1}(0), x_{1,2}(0)\right] = [0.1, 0.1]^{\mathrm{T}}$, $\bar{x}_{2,2}(0) = \left[x_{2,1}(0), x_{2,2}(0)\right] = [0.2, 0.05]^{\mathrm{T}}$, $\bar{x}_{3,2}(0) = \left[x_{3,1}(0), x_{3,2}(0)\right] = [0.2, 0.1]^{\mathrm{T}}$, $\bar{x}_{4,2}(0) = \left[x_{3,1}(0), x_{3,2}(0)\right] = [0.4, 0.1]^{\mathrm{T}}$, with the reference signal being $y_d = 0.5\sin(t)$. In the predefined time control, the remaining parameters are set as $T_p = 0.2s$, $\eta = 0.5$, $\upsilon_{1,2} = 100$, $\upsilon_{2,2} = 100$, $\upsilon_{3,2} = 100$,$\upsilon_{4,2} = 10$, $c_{1,1} = 20$, $c_{1,2} = c_{2,2} = c_{3,2} = c_{4,2} = 1$, $c_{2,1} = c_{3,1} = c_{4,1} = 10$, $c_{4,1} = 5$, $\varepsilon_{1,1} = \varepsilon_{1,2} = 0.01$, $\varepsilon_{1,3} = 0.1$, $\varepsilon_{1,4} = 0.001$, $p_{1,1} = 0.0005$, $p_{1,2} = p_{2,2} = p_{3,2} = p_{4,2} = 1$, $p_{2,1} = 0.002$, $p_{3,1} = 0.0005$, $p_{4,1} = 0.005$, $k_{1,1} = k_{2,1} = k_{3,1} = k_{4,1} = 1$, $r_a = -30$, $r_b = 20$, $a_{1\,m} = a_{2\,m} = a_{3\,m} = a_{4\,m} = 2$. The finite-time controller is designed as $u_{i,n} = -c_{i,n}z_{i,n}^{2\sigma-1} - r_{i,n}\hat{\theta}_{i,n}^{\mathrm{T}}\xi_{i,n}$ with parameters $\sigma = 199/201$, $c_{1,1} = 80$, $c_{1,2} = 15$, $c_{1,3} = 8$, $c_{1,4} = 5$, $c_{2,1} = c_{2,3} = 10$, $c_{2,2} = 20$, $c_{2,4} = 12$, $r_{1,1} = r_{1,2} = 10$, $r_{1,3} = r_{1,4} = 5$, $r_{2,1} = r_{2,2} = 2$, $r_{2,3} = 5$, $r_{2,4} = 8$.

The simulation results are shown in Fig. 13. Figure 13a presents the tracking curve under predefined time control, while Fig. 13b shows the tracking curve under finite-time control. From Fig. 13, it is evident that, under larger initial conditions, the finite-time control performs worse in terms of both tracking speed and accuracy. In contrast, the proposed control scheme is still able to meet the predefined time control requirements and achieve fast tracking of the agent, even with larger initial conditions.

Based on the aforementioned simulation results, it can be observed that the proposed control scheme maintains robust performance in multi-agent systems with nonlinear dynamics, external disturbances, and saturation constraints. Additionally, it effectively avoids issues such as computational explosion and control jitter, thus advancing the research on nonlinear multi-agent systems.

### 4.4 The performance for a generic trapezoidal leader

To verify whether the control scheme proposed in this paper is applicable to a broader range of scenarios, we validated the system's tracking performance under a general trapezoidal leader. The velocity signal of the trapezoidal leader is selected as follows

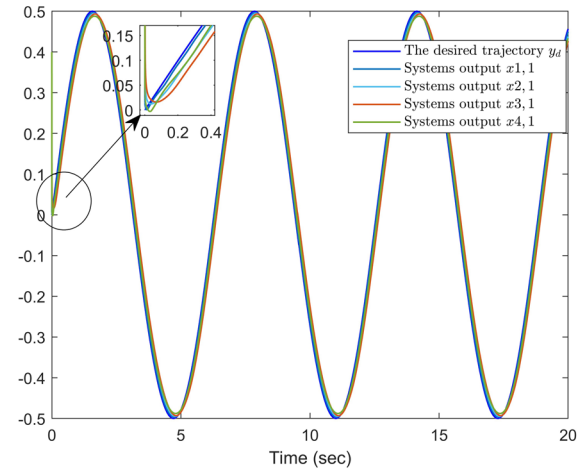


(a) Tracking curve of the proposed method

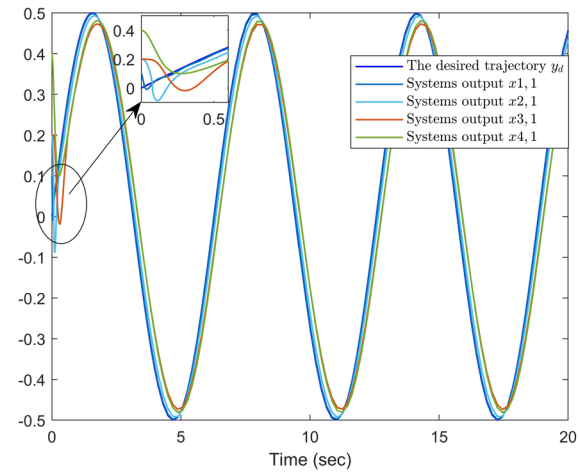


(b) Tracking curve of finite-time control method

**Fig. 13** Comparison of predefined time and finite time

$$v = \begin{cases} at, & 0 \le t < t_{acc} \\ v_{\max}, & t_{acc} \le t \le t_{slow} \\ v_{\max} - s\,(t - t_{slow}), & t_{slow} \le t < T \end{cases} \tag{79}$$

where $a = 0.2m/s^2$ represents acceleration, $s = 0.1m/s^2$ represents deceleration, $v_{\max} = 0.4m/s$ represents maximum velocity, $t_{acc} = 2s$ represents accel-

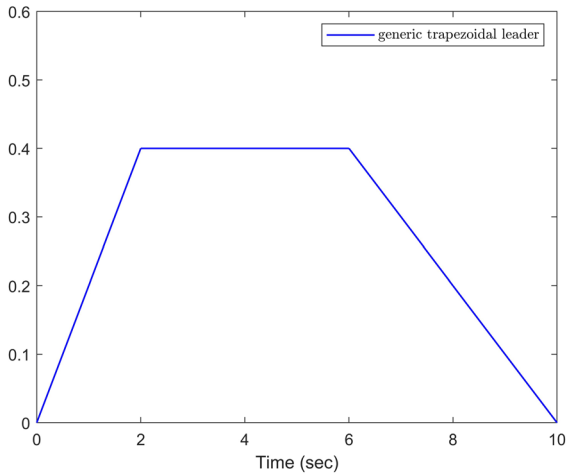


**Fig. 14** Generic trapezoidal leader's signal

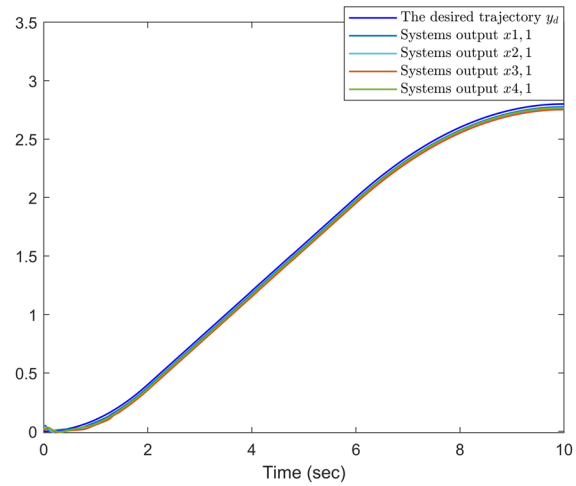


**Fig. 15** The tracking curve under the trapezoidal leader

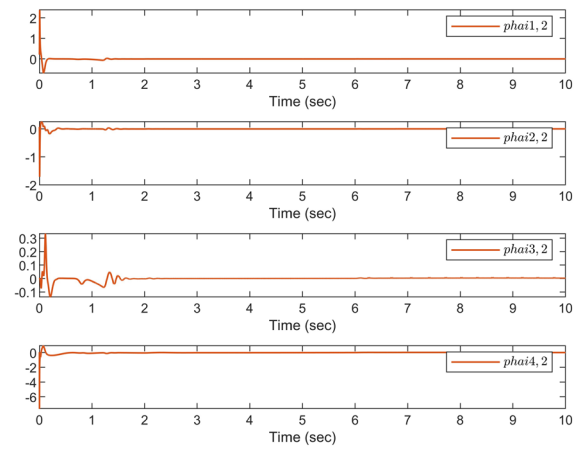


**Fig. 16** The filtering error under the trapezoidal leader

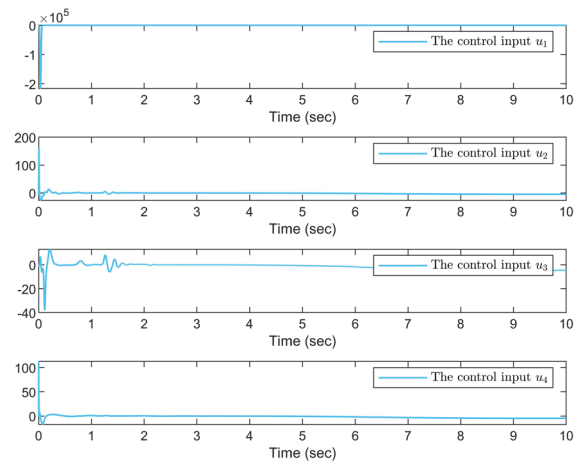


**Fig. 17** The virtual control input under the trapezoidal leader

eration time, $t_{slow} = 6\,s$ represents deceleration time, and $T = 10\,s$ represents maximum time. Below is a schematic of the trapezoidal leader's velocity signal.

As shown in Fig. 14, from 0 to 2 s, the leader is in the acceleration phase, with the velocity increasing from $0m/s$ to $0.4m/s$. From 2 to 6 s, the leader moves at a constant velocity, maintaining the maximum speed $v_{\max} = 0.4m/s$. From 6 to 10 s, the leader enters the deceleration phase, with the velocity decreasing from $0.4m/s$ to $0m/s$.

The initial conditions are set as $\bar{x}_{1,2}(0) = \left[x_{1,1}(0), x_{1,2}(0)\right] = [0.05, 0.2]^{\mathrm{T}}, \bar{x}_{2,2}(0) = \left[x_{2,1}(0), x_{2,2}(0)\right] = [0.02, 0.1]^{\mathrm{T}}, \bar{x}_{3,2}(0) = \left[x_{3,1}(0), x_{3,2}(0)\right] = [0.01, 0.2]^{\mathrm{T}}, \bar{x}_{4,2}(0) = \left[x_{3,1}(0), x_{3,2}(0)\right] = [0.02, 0.1]^{\mathrm{T}}$, and the remaining parameters are set as $p_{1,1} = 0.005$, $p_{2,1} = p_{3,1} = 0.002$, $p_{4,1} = 0.0005$. The other simulation conditions and parameters are the same as numerical examples in the previous case.

The simulation results are shown below. Figure 15 represents the tracking curve under the trapezoidal leader, Fig. 16 shows the filtering error under the trapezoidal leader, Fig. 17 illustrates the filtering error under the trapezoidal leader, and Fig. 18 displays the filtering error under the trapezoidal leader. From Fig. 15 to Fig. 18, it can be seen that the control scheme proposed in this paper for nonlinear multi-agent systems with input saturation still exhibits good tracking performance when the leader is a general trapezoidal leader.

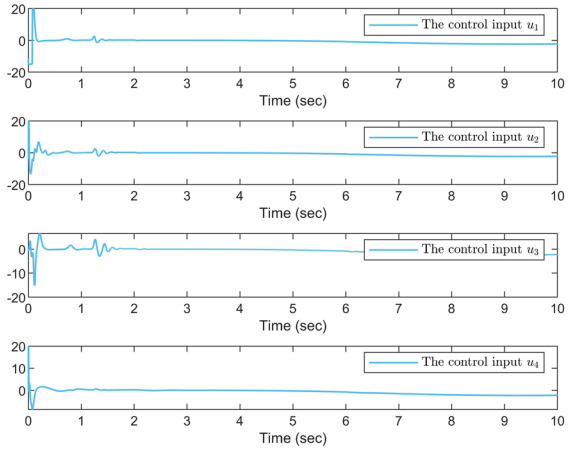


**Fig. 18** The saturated input under the trapezoidal leader

## 5 Conclusion

This paper investigates a predefined time command-filtered control method for strict-feedback NMASs with input saturation, based on adaptive multi-dimensional Taylor network (MTN). First, a novel practical predefined time stability (PPTS) theory is proposed, building on the existing predefined time control framework. Subsequently, combining the PPTS theory and hyperbolic tangent functions, a practical predefined time command filter suitable for NMASs is designed. This filter not only satisfies predefined time stability requirements but also effectively avoids control singularities and computational explosions, significantly improving system stability and practical engineering applicability. To address input saturation issues, a novel injective and differentiable function is constructed to approximate the nonlinear behavior of the saturation function. Combined with MTN to approximate complex system nonlinearities, this approach simplifies the controller design process. The proposed strategy ensures boundedness of all signals in the closed-loop system and achieves rapid convergence of tracking errors to a small neighborhood of the origin within the predefined time, meeting high-accuracy control requirements. The effectiveness and practicality of the proposed control scheme are validated through numerical simulations, two practical examples, and comparative experiments. Results demonstrate its superior performance in handling input saturation, nonlinearity, and external disturbances.

In future research on theoretical studies, we will explore the combination of predefined time control with asymptotic tracking control, aiming to achieve asymptotic convergence of tracking errors within predefined time approach, and in future research on practical systems, we will incorporate collision avoidance mechanisms and safety distance constraints into the control framework, particularly for systems where physical constraints or safety requirements are critical. Such modifications will ensure that the proposed control method can be effectively applied to real-world scenarios involving mobile agents, such as drones, while maintaining stability and safety.

**Funding** This work was supported by the Shandong Provincial Natural Science Foundation, China (No. ZR2020QF055).

**Data Availability Statement** Data sharing is not applicable to this article as no datasets were generated or analysed during the current study.

**Declarations**

**Conflict of interest** The authors declare that he has no conflict of interest.

## References

1. Yang, T., Yi, X.L., Wu, J.F., Yuan, Y., Wu, D., Meng, Z.Y., Hong, Y.G., Wang, H., Lin, Z.L., Johansson, K.H.: A survey of distributed optimization. Ann. Rev. Control **47**, 278–305 (2019). https://doi.org/10.1016/j.arcontrol.2019.05.006
2. McArthur, S.D., Davidson, E.M., Catterson, V.M., Dimeas, A.L., Hatziargyriou, N.D., Ponci, F., Funabashi, T.: Multi-agent systems for power engineering applications-part i: Concepts, approaches, and technical challenges. IEEE Trans. Power Syst. **22**(4), 1743–1752 (2007). https://doi.org/10.1109/TPWRS.2007.908471
3. Oliveira, E., Fischer, K., Stepankova, O.: Multi-agent systems: which research for which applications. Robot. Auton. Syst. **27**(1–2), 91–106 (1999). https://doi.org/10.1016/S0921-8890(98)00085-2
4. Khoo, S.Y., Xie, L.H., Man, Z.H.: Robust finite-time consensus tracking algorithm for multirobot systems. IEEE/ASME Trans. Mechatron. **14**(2), 219–228 (2009). https://doi.org/10.1109/TMECH.2009.2014057
5. Qiu, Z.R., Xie, L.H., Hong, Y.G.: Quantized leaderless and leader-following consensus of high-order multi-agent systems with limited data rate. IEEE Trans. Autom. Control **61**(9), 2432–2447 (2015). https://doi.org/10.1109/TAC.2015.2495579
6. Qin, J.H., Yu, C.B., Anderson, B.D.: On leaderless and leader-following consensus for interacting clusters of second-order multi-agent systems. Automatica **74**, 214–221 (2016). https://doi.org/10.1016/j.automatica.2016.07.008

7. Gao, Y.P., Liu, B., Yu, J.Y., Ma, J.W., Jiang, T.Q.: Consensus of first-order multi-agent systems with intermittent interaction. Neurocomputing **129**, 273–278 (2014). https://doi.org/10.1016/j.neucom.2013.09.031
8. Du, H.B., Li, S.H., Shi, P.: Robust consensus algorithm for second-order multi-agent systems with external disturbances. Int. J. Control **85**(12), 1913–1928 (2012). https://doi.org/10.1080/00207179.2012.713515
9. Wang, Y.J., Song, Y.D.: Leader-following control of high-order multi-agent systems under directed graphs: Prespecified finite time approach. Automatica **87**, 113–120 (2018). https://doi.org/10.1016/j.automatica.2017.09.017
10. Wu, W., Tong, S.C.: Fuzzy adaptive consensus control for nonlinear multiagent systems with intermittent actuator faults. IEEE Trans. Cybernetics **53**(5), 2969–2979 (2021). https://doi.org/10.1109/TCYB.2021.3123788
11. Lei, J.Y., Li, Y.X., Tong, S.C.: Fuzzy adaptive distributed optimization of uncertain multiagent systems with time-varying delays. IEEE Trans. Fuzzy Syst. **32**(11), 6125–6135 (2024). https://doi.org/10.1109/TFUZZ.2024.3441008
12. Li, K.W., Song, L.L., Li, Y.M.: Fuzzy adaptive resilient output control for nonlinear multi-agent systems under byzantine agents. IEEE Trans. Automation Sci. Eng. (2024). https://doi.org/10.1109/TASE.2024.3488820
13. Wu, L.B., Park, J.H., Xie, X.P., Ren, Y.W., Yang, Z.C.: Distributed adaptive neural network consensus for a class of uncertain nonaffine nonlinear multi-agent systems. Nonlinear Dyn. **100**, 1243–1255 (2020). https://doi.org/10.1007/s11071-020-05599-2
14. Liu, Z.J., Lu, Z.Q., Zhao, Z.J., Efe, M.Ö., Hong, K.-S.: Single parameter adaptive neural network control for multi-agent deployment with prescribed tracking performance. Automatica **156**, 111207 (2023). https://doi.org/10.1016/j.automatica.2023.111207
15. Lu, L.T., Zhu, S.L., Wang, D.M., Han, Y.Q.: Predefined-time adaptive consensus control for nonlinear multi-agent systems with input quantization and actuator faults. Nonlinear Dyn. **112**(16), 14215–14234 (2024)
16. Lu, L.T., Zhu, S.L., Wang, D.M., Han, Y.Q.: Distributed adaptive fault-tolerant control with prescribed performance for nonlinear multiagent systems. Commun. Nonlinear Sci. Num. Simulation **138**, 108222 (2024). https://doi.org/10.1016/j.cnsns.2024.108222
17. Swaroop, D., Hedrick, J.K., Yip, P.P., Gerdes, J.C.: Dynamic surface control for a class of nonlinear systems. IEEE Trans. Autom. Control **45**(10), 1893–1899 (2000). https://doi.org/10.1109/TAC.2000.880994
18. Farrell, J.A., Polycarpou, M., Sharma, M., Dong, W.J.: Command filtered backstepping. IEEE Trans. Autom. Control **54**(6), 1391–1395 (2009). https://doi.org/10.1109/TAC.2009.2015562
19. Grujic, L., Siljak, D.: Asymptotic stability and instability of large-scale systems. IEEE Trans. Autom. Control **18**(6), 636–645 (1973). https://doi.org/10.1109/TAC.1973.1100422
20. Huang, X.Q., Lin, W., Yang, B.: Global finite-time stabilization of a class of uncertain nonlinear systems. Automatica **41**(5), 881–888 (2005). https://doi.org/10.1016/j.automatica.2004.11.036
21. Yin, J.L., Khoo, S.Y., Man, Z.H., Yu, X.H.: Finite-time stability and instability of stochastic nonlinear systems. Automatica **47**(12), 2671–2677 (2011). https://doi.org/10.1016/j.automatica.2011.08.050
22. Polyakov, A.: Nonlinear feedback design for fixed-time stabilization of linear control systems. IEEE Trans. Autom. Control **57**(8), 2106–2110 (2012). https://doi.org/10.1109/TAC.2011.2179869
23. Sánchez-Torres, J.D., Gómez-Gutiérrez, D., López, E., Loukianov, A.G.: A class of predefined-time stable dynamical systems. IMA J. Math. Control Inform. **35**, 1–29 (2018). https://doi.org/10.1093/imamci/dnx004
24. Hua, C.C., Ning, P.J., Li, K.: Adaptive prescribed-time control for a class of uncertain nonlinear systems. IEEE Trans. Autom. Control **67**(11), 6159–6166 (2022). https://doi.org/10.1109/TAC.2021.3130883
25. Sui, S., Chen, C.L.P., Tong, S.C.: Command filter-based predefined time adaptive control for nonlinear systems. IEEE Trans. Autom. Control **69**(11), 7863–7870 (2024). https://doi.org/10.1109/TAC.2024.3399998
26. Wang, H.Q., Tong, M., Zhao, X.D., Niu, B., Yang, M.: Predefined-time adaptive neural tracking control of switched nonlinear systems. IEEE Trans. Cybernetics **53**(10), 6538–6548 (2023). https://doi.org/10.1109/TCYB.2022.3204275
27. Pan, Y.N., Ji, W.Y., Lam, H.-K., Cao, L.: An improved predefined-time adaptive neural control approach for nonlinear multiagent systems. IEEE Trans. Autom. Sci. Eng. **21**(4), 6311–6320 (2024). https://doi.org/10.1109/TASE.2023.3324397
28. Ma, J.W., Zhang, H.G., Zhang, J., Guo, X.Y.: Predefined-time control for multi-agent systems with input saturation: An improved dynamic surface control scheme. IEEE Trans. Automation Sci. Eng. **22**, 3661–3670 (2025). https://doi.org/10.1109/TASE.2024.3398629
29. Ni, J.K., Liu, L., Tang, Y., Liu, C.X.: Predefined-time consensus tracking of second-order multiagent systems. IEEE Trans. Syst. Man Cybernetics: Syst. **51**(4), 2550–2560 (2021). https://doi.org/10.1109/TSMC.2019.2916257
30. Wen, C.Y., Zhou, J., Liu, Z.T., Su, H.Y.: Robust adaptive control of uncertain nonlinear systems in the presence of input saturation and external disturbance. IEEE Trans. Autom. Control **56**(7), 1672–1678 (2011). https://doi.org/10.1109/TAC.2011.2122730
31. Chen, B.M., Lee, T.H., Peng, K., Venkataramanan, V.: Composite nonlinear feedback control for linear systems with input saturation: theory and an application. IEEE Trans. Autom. Control **48**(3), 427–439 (2003). https://doi.org/10.1109/TAC.2003.809148
32. Grimm, G., Hatfield, J., Postlethwaite, I., Teel, A.R., Turner, M.C., Zaccarian, L.: Antiwindup for stable linear systems with input saturation: an lmi-based synthesis. IEEE Trans. Autom. Control **48**(9), 1509–1525 (2003). https://doi.org/10.1109/TAC.2003.816965
33. Liu, Z., Zhao, Y., Zhang, O.Y., Chen, W.L., Wang, J.H., Gao, Y.B., Liu, J.X.: A novel faster fixed-time adaptive control for robotic systems with input saturation. IEEE Trans. Industr. Electron. **71**(5), 5215–5223 (2024). https://doi.org/10.1109/TIE.2023.3281701
34. Shi, X.N., Zhou, Z.G., Zhou, D., Li, R.F.: Event-triggered fixed-time adaptive trajectory tracking for a class of uncertain nonlinear systems with input saturation. IEEE Trans. Circuits Syst. II Express Briefs **68**(3), 983–987 (2021). https://doi.org/10.1109/TCSII.2020.3018194

35. Xie, H.Z., Zong, G.D., Yang, D., Zhao, X.D., Yi, Y.: Flexible-fixed-time-performance-based adaptive asymptotic tracking control of switched nonlinear systems with input saturation. IEEE Trans. Autom. Sci. Eng. **21**(4), 6371–6382 (2024). https://doi.org/10.1109/TASE.2023.3324953
36. Gao, Y.F., Sun, X.M., Wen, C.Y., Wang, W.: Adaptive tracking control for a class of stochastic uncertain nonlinear systems with input saturation. IEEE Trans. Autom. Control **62**(5), 2498–2504 (2017). https://doi.org/10.1109/TAC.2016.2600340
37. Li, N., Du, Y., Wang, D.M., Zhu, S.L., Han, Y.Q.: Adaptive decentralized prescribed performance control for a class of large-scale stochastic nonlinear systems subject to input saturation and full state constraints. Int. J. Adapt. Control Signal Process. **37**(9), 2451–2471 (2023). https://doi.org/10.1002/acs.3647
38. Song, Z.B., Li, P., Wang, Z., Huang, X., Liu, W.H.: Adaptive tracking control for switched uncertain nonlinear systems with input saturation and unmodeled dynamics. IEEE Trans. Circuits Syst. II Express Briefs **67**(12), 3152–3156 (2020). https://doi.org/10.1109/TCSII.2020.2966298
39. Yang, T., Meng, Z.Y., Dimarogonas, D.V., Johansson, K.H.: Global consensus for discrete-time multi-agent systems with input saturation constraints. Automatica **50**(2), 499–506 (2014). https://doi.org/10.1016/j.automatica.2013.11.008
40. ur Rehman, A., Rehan, M., Riaz, M., Abid, M., Iqbal, N.: Consensus tracking of nonlinear multi-agent systems under input saturation with applications: A sector-based approach. ISA Trans. **107**, 194–205 (2020). https://doi.org/10.1016/j.isatra.2020.07.030
41. Yu, J.J., Yu, S.H., Yan, Y.: Fixed-time stability of stochastic nonlinear systems and its application into stochastic multi-agent systems. IET Control Theory Appl. **15**(1), 126–135 (2021). https://doi.org/10.1049/cth2.12040
42. Wang, H.Q., Chen, B., Liu, K., Liu, X., Lin, C.: Adaptive neural tracking control for a class of nonstrict-feedback stochastic nonlinear systems with unknown backlash-like hysteresis. IEEE Trans. Neural Networks Learning Syst. **25**(5), 947–958 (2014). https://doi.org/10.1109/TNNLS.2013.2283879
43. Dong, W.J., Farrell, J.A., Polycarpou, M.M., Djapic, V., Sharma, M.: Command filtered adaptive backstepping. IEEE Trans. Control Syst. Technol. **20**(3), 566–580 (2012). https://doi.org/10.1109/TCST.2011.2121907
44. Shen, Q.K., Jiang, B., Shi, P., Zhao, J.: Cooperative adaptive fuzzy tracking control for networked unknown nonlinear multiagent systems with time-varying actuator faults. IEEE Trans. Fuzzy Syst. **22**(3), 494–504 (2014). https://doi.org/10.1109/TFUZZ.2013.2260757
45. SÃ¡nchez-Torres, J.D., Sanchez, E.N., Loukianov, A.G.: Predefined-time stability of dynamical systems with sliding modes, 5842–5846 (2015) https://doi.org/10.1109/ACC.2015.7172255
46. Sun, Y., Wang, F., Liu, Z., Zhang, Y., Chen, C.L.P.: Fixed-time fuzzy control for a class of nonlinear systems. IEEE Trans. Cybernetics **52**(5), 3880–3887 (2022). https://doi.org/10.1109/TCYB.2020.3018695
47. Yan, H.S., Han, Y.Q.: Decentralized adaptive multi-dimensional taylor network tracking control for a class of large-scale stochastic nonlinear systems. Int. J. Adapt. Control Signal Process. **33**(4), 664–683 (2019). https://doi.org/10.1002/acs.2978
48. Zhang, J.J., Yan, H.S.: Mtn optimal control of mimo non-affine nonlinear time-varying discrete systems for tracking only by output feedback. J. Franklin Inst. **356**(8), 4304–4334 (2019). https://doi.org/10.1016/j.jfranklin.2019.03.008